AMERICAN SOCIETY FOR MICROBIOLOGY | Journal of Virology

Editor's Pick | Virology | Full-Length Text

Oxidative stress sensor Keap1 recognizes HBx protein to activate the Nrf2/ARE signaling pathway, thereby inhibiting hepatitis B virus replication

Adi Ariffianto,[1,2] Lin Deng,[1] Takayuki Abe,[1] Chieko Matsui,[1] Masahiko Ito,[3] Akihide Ryo,[4] Hussein Hassan Aly,[5] Koichi Watashi,[5,6] Tetsuro Suzuki,[3] Masashi Mizokami,[7] Yoshiharu Matsuura,[8,9] Ikuo Shoji[1]

AUTHOR AFFILIATIONS See affiliation list on p. 32.

ABSTRACT Hepatitis B virus (HBV) infection promotes reactive oxygen species production while paradoxically inducing the expression of antioxidant enzymes. HBV-induced disorders of redox homeostasis are closely associated with the development of hepatic diseases. However, the molecular mechanisms underlying the HBV-induced antioxidant response are poorly understood. The NF-E2-related factor 2 (Nrf2)/antioxidant response element (ARE) signaling pathway is an intrinsic defense mechanism against oxidative stress. We here aim to elucidate the role of the Nrf2/ARE signaling pathway in the HBV life cycle. ARE-driven reporter assays revealed that expression of HBV X protein (HBx), but not HBV core, large HBV surface, or HBV polymerase, strongly enhanced ARE-luciferase activity, suggesting that HBx plays an important role in the HBV-induced antioxidant response. Knockdown of Nrf2 resulted in a marked decrease in HBx-induced ARE-luciferase activity. Immunoblot analysis and immunofluorescence staining suggested that HBx activates Nrf2 by increasing Nrf2 protein levels and enhancing Nrf2 nuclear localization. The oxidative stress sensor Kelch-like ECH-associated protein 1 (Keap1) is required for the ubiquitin-dependent degradation of Nrf2. Coimmunoprecipitation analysis revealed that HBx interacted with Keap1, suggesting that HBx competes with Nrf2 for interaction with Keap1. A cell-based ubiquitylation assay showed that HBx promoted polyubiquitylation of Nrf2 via K6-linked polyubiquitin chains, and that this action may be associated with Nrf2 stabilization. A chromatin immunoprecipitation assay suggested that Nrf2 interacts with the HBV core promoter. Overexpression of Nrf2 strongly suppressed HBV core promoter activity, resulting in a marked reduction in viral replication. Based on the above, we propose that Keap1 recognizes HBx to activate the Nrf2/ARE signaling pathway upon HBV infection, thereby inhibiting HBV replication.

IMPORTANCE The Kelch-like ECH-associated protein 1 (Keap1)/NF-E2-related factor 2 (Nrf2)/antioxidant response element (ARE) signaling pathway is one of the most important defense mechanisms against oxidative stress. We previously reported that a cellular hydrogen peroxide scavenger protein, peroxiredoxin 1, a target gene of transcription factor Nrf2, acts as a novel HBV X protein (HBx)-interacting protein and negatively regulates hepatitis B virus (HBV) propagation through degradation of HBV RNA. This study further demonstrates that the Nrf2/ARE signaling pathway is activated during HBV infection, eventually leading to the suppression of HBV replication. We provide evidence suggesting that Keap1 interacts with HBx, leading to Nrf2 activation and inhibition of HBV replication via suppression of HBV core promoter activity. This study raises the possibility that activation of the Nrf2/ARE signaling pathway is a potential therapeutic strategy against HBV. Our findings may contribute to an improved understanding of the negative regulation of HBV replication by the antioxidant response.

Editor J.-H. James Ou, University of Southern California, Los Angeles, California, USA

Address correspondence to Ikuo Shoji, ishoji@med.kobe-u.ac.jp.

The authors declare no conflict of interest.

See the funding table on p. 32.

Received 21 August 2023
Accepted 22 August 2023
Published 6 October 2023

KEYWORDS hepatitis B virus, HBx, Keap1/Nrf2/ARE

Chronic hepatitis B virus (HBV) infection is a leading cause of severe liver diseases, including cirrhosis and primary hepatocellular carcinoma (1). Despite the availability of an effective prophylactic vaccine, HBV infection remains a major public health problem worldwide, with approximately 290 million chronically infected people globally and 1.5 million new infections each year (2). Current nucleos(t)ide- and PEGylated interferon α-based therapies can inhibit HBV replication but rarely achieve a functional cure (3).

HBV is a small, enveloped DNA virus that belongs to the Hepadnaviridae family. The HBV genome is a partially double-stranded circular DNA of approximately 3.2 kb in length and encodes several different viral proteins. These include HBV surface antigen (HBsAg; of which there are three forms: large, medium, and small), HBV core antigen (HBcAg), HBV envelope antigen (HBeAg), HBV polymerase (pol), and HBV X protein (HBx) (4).

Oxidative stress plays an important role in the pathogenesis of chronic diseases, including diabetes, cancer, and neurodegenerative diseases (5–7). An imbalance between oxidants and antioxidants leads to a disruption of redox signaling and cellular damage (8). However, cells also possess effective antioxidant defense mechanisms to combat such disruption and maintain cellular homeostasis. The NF-E2-related factor 2 (Nrf2)/antioxidant response element (ARE) signaling pathway controls the expression of genes involved in protecting cells from oxidative damage (9, 10). Nrf2 abundance within the cell is tightly regulated by Kelch-like ECH-associated protein 1 (Keap1), an adaptor subunit of a Cullin 3 (Cul3)-based ubiquitin ligase. Under unstressed conditions, Keap1 binds to Nrf2 in the cytoplasm and promotes the ubiquitylation and proteasomal degradation of Nrf2. Upon exposure to reactive oxygen species (ROS), Keap1 is oxidized at reactive cysteine residues, resulting in Keap1-Cul3 complex inactivation and Nrf2 stabilization. Nrf2 translocates to the nucleus, where it heterodimerizes with small musculoaponeurotic fibrosarcoma oncogene homolog (sMaf) proteins. Nrf2-sMaf complexes bind to the AREs located in the promoter region of Nrf2 target genes and activate their transcription (11, 12).

The relationship between HBV and oxidative stress has been studied. ROS levels are known to be increased in the liver and blood of HBV-infected patients. The accumulation of ROS is related to the severity of hepatic disease (13–17). HBV-mediated ROS production is triggered by HBV replication (18) and three viral proteins: HBx (19–21), HBsAg (22), and HBcAg (23). Meanwhile, HBV infection induces the expression of antioxidant enzymes such as NAD(P)H quinone dehydrogenase 1 (NQO1) and γ-glutamyl cysteine synthetase via activation of the Nrf2/ARE signaling pathway. HBx and large HBsAg (LHBs) have the potential to activate Nrf2/ARE-dependent gene expression (24). However, the functional relevance of the Nrf2/ARE signaling pathway for HBV replication is largely unknown.

In this study, we demonstrate that Keap1 interacts with HBx protein to activate the Nrf2/ARE signaling pathway upon HBV infection, leading to suppression of HBV replication via inhibition of HBV core promoter activity. Thus, we propose that the Keap1/Nrf2/ARE signaling pathway negatively regulates HBV propagation to protect the host cells.

RESULTS

The HBx protein plays an important role in the HBV-induced antioxidant response

To investigate whether HBV infection affects the antioxidant response pathway, we performed RNA-seq analysis on HBV-infected HepG2-hNTCP-C4 cells and mock-infected control cells at 12 days postinfection (dpi). We found significant changes in the expression levels of 1,590 genes upon HBV infection, with 757 genes upregulated and 833 genes downregulated among the 21,449 genes analyzed (Fig. 1A, upper panel).

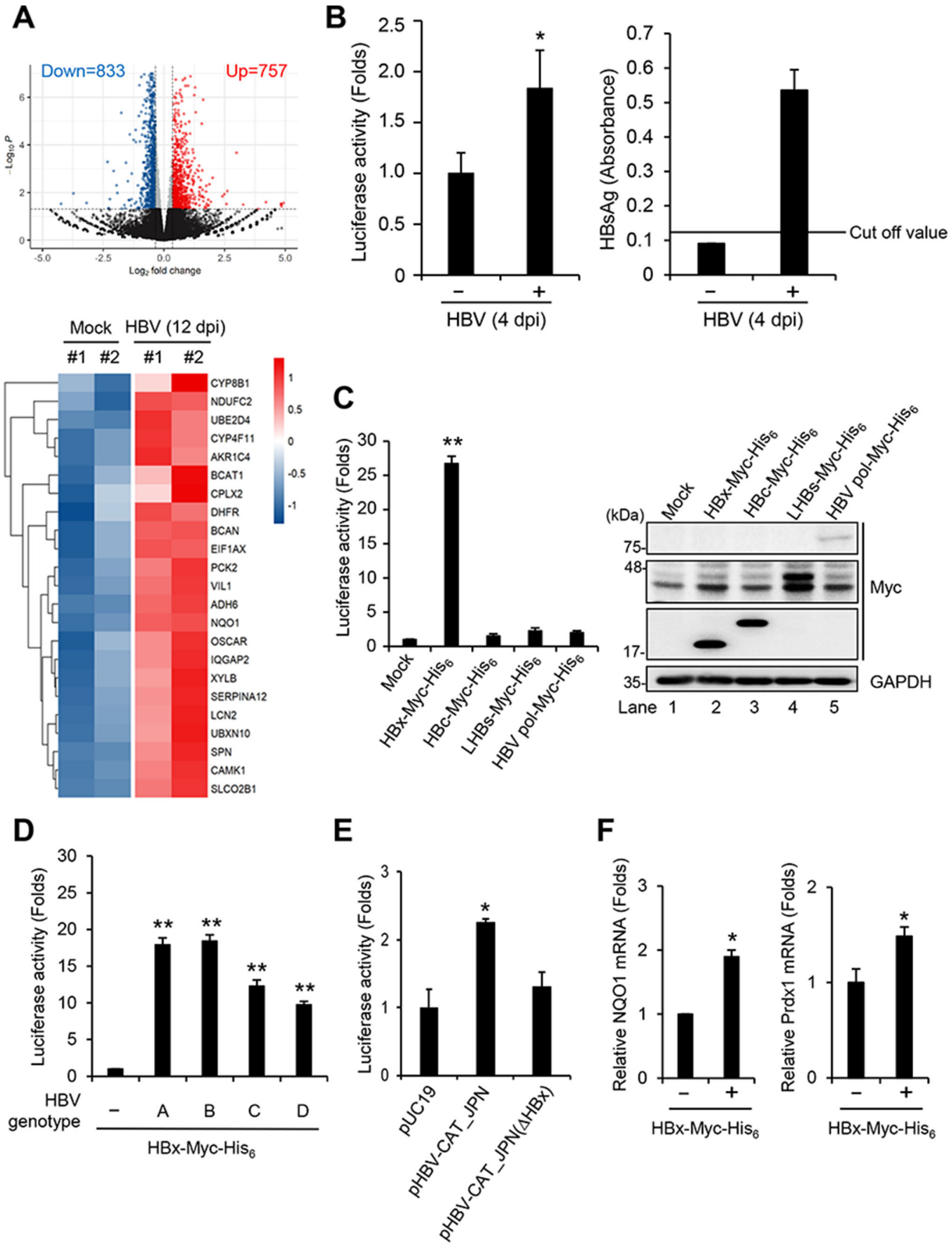

FIG 1 HBx protein plays an important role in the HBV-induced antioxidant response. (A) HepG2-hNTCP-C4 cells were infected with HBV at 40,000 genome equivalents (GEq)/cell. At 12 dpi, total RNA was isolated from two sets of HBV-infected cells and mock-infected control cells (referred to as #1 and #2), followed by RNA-Seq analysis. The volcano plot displayed differentially expressed genes (top panel). The x-axis represented the $\log_2$(fold change), and the y-axis represented the significance of gene expression in HBV-infected cells compared to that in mock-infected cells. Each dot represented one gene, with

(Continued on next page)

FIG 1 (Continued)

red, blue, or black dots indicating genes with significantly upregulated expression values, downregulated expression values, or other genes, respectively. The heat map represented the upregulated Nrf2-target genes and/or antioxidant genes in HBV-infected cells compared to the mock-infected control cells (bottom panel). (B) HepG2-hNTCP-C4 cells were infected with HBV at 40,000 GEq/cell. At 24 h after inoculation, the cells were transfected with the ARE-luciferase reporter gene pGL4.37[luc2P/ARE/Hygro] and harvested at 4 dpi. ARE-luciferase activity was measured and normalized to *Renilla* activity (left panel). The level of HBsAg in the culture supernatant of HBV-infected HepG2-hNTCP-C4 cells was measured by enzyme-linked immunosorbent assay (right panel). The cut-off absorbance value was 0.12 (negative control absorbance plus 0.025). (C, D, and E) HepG2 cells were transfected with pGL4.37[luc2P/ARE/Hygro] together with Myc-His_6-tagged HBx, HBc, LHBs, or HBV pol expression plasmids (C), Myc-His_6-tagged HBx expression plasmids derived from HBV genotypes A, B, C, or D (D), and either pUC19-HBV-C-AT_JPN or pUC19-HBV-C-AT_JPN(ΔHBx) (E). At 48 h after transfection, the cells were harvested. ARE-luciferase activity was measured and normalized to *Renilla* activity. The expression levels of Myc-His_6-tagged HBx, HBc, LHBs, and HBV pol in cell lysates were analyzed by immunoblotting with anti-c-Myc monoclonal antibody (C, right panel). The level of glyceraldehyde-3-phosphate dehydrogenase (GAPDH) served as a loading control. (F) HepG2 cells were transfected with pEF1A-HBx-Myc-His_6. At 48 h after transfection, the total RNA was extracted, and the mRNA levels of NQO1 and peroxiredoxin 1 were quantitated by real-time reverse transcription-PCR. The data represent the means ± SEM of data from three independent experiments, and the value for the control cells was arbitrarily expressed as 1.0. *$P < 0.05$, **$P < 0.01$, compared with the controls.

Moreover, among the upregulated genes, we identified 23 genes that are Nrf2-target genes and/or associated with antioxidant activities (Fig. 1A, lower panel). Notably, several phase I detoxification enzymes were identified, including aldo-keto reductase family 1 member C4, cytochrome P450 family 8 subfamily B member 1, and cytochrome P450 family 4 subfamily F member 11, as well as the phase II detoxification enzyme NQO1 (Fig. 1A). These genes were all recognized as Nrf2-target genes and exhibited increased expression in response to HBV infection. These results suggest that HBV infection induces an Nrf2-mediated antioxidant response and detoxification process.

To further investigate the effect of HBV infection on the antioxidant response pathway, HBV-infected HepG2-hNTCP-C4 cells were transfected with the ARE-driven luciferase gene construct pGL4.37[luc2P/ARE/Hygro]. HBsAg in the culture supernatant was quantified by enzyme-linked immunosorbent assay (ELISA) (Fig. 1B, right panel). This result indicates that HBsAg was efficiently released in the supernatant from HBV-infected HepG2-hNTCP-C4 cells at 4 dpi. ARE-luciferase activity was significantly increased in HBV-infected cells at 4 dpi compared to that in mock-infected control cells (Fig. 1B, left panel), suggesting that HBV infection induces an antioxidant response.

To determine which HBV protein is involved in the enhancement of HBV-mediated ARE-luciferase activity, HepG2 cells were transfected with pGL4.37[luc2P/ARE/Hygro] together with Myc-His_6-tagged HBV viral protein (HBx, HBc, LHBs, or HBV pol)-expression plasmids. The luciferase reporter assay showed that HBx more strongly enhanced ARE-luciferase activity than the other viral proteins (Fig. 1C, left panel). The immunoblot analysis showed the expression levels of Myc-His_6-tagged HBx, HBc, LHBs, and HBV pol (Fig. 1C, right panel). Moreover, the ARE-luciferase assay revealed that HBx proteins derived from HBV genotypes A, B, C, and D markedly enhanced ARE-luciferase activities (Fig. 1D). To further determine the role of HBx in HBV-induced ARE-luciferase activity, HepG2 cells were co-transfected with pGL4.37[luc2P/ARE/Hygro] together with either pUC19-HBV-C-AT_JPN or pUC19-HBV-C-AT_JPN(ΔHBx). The luciferase assay revealed that HBV-C-AT_JPN significantly enhanced ARE-luciferase activity compared to the control, whereas HBV-C-AT_JPN (ΔHBx) failed to enhance ARE-luciferase activity (Fig. 1E). These results suggest that HBx participates in HBV-induced ARE-luciferase activity. We further verified the role of HBx in the ARE-dependent expression of the NQO1 and peroxiredoxin 1 (Prdx1) genes in HepG2 cells. A real-time reverse transcription-PCR (RT-PCR) assay showed that HBx significantly enhanced the mRNA levels of NQO1 (Fig. 1F, left panel) and Prdx1 (Fig. 1F, right panel). These results suggest that the HBx protein plays an important role in the HBV-induced antioxidant response.

Nrf2 is involved in the HBx-induced antioxidant response

To determine whether Nrf2 is involved in HBx-induced ARE-luciferase activity, HepG2 cells were co-transfected with pEF1A-HBx-Myc-His_6 and pGL4.37[luc2P/ARE/Hygro] in

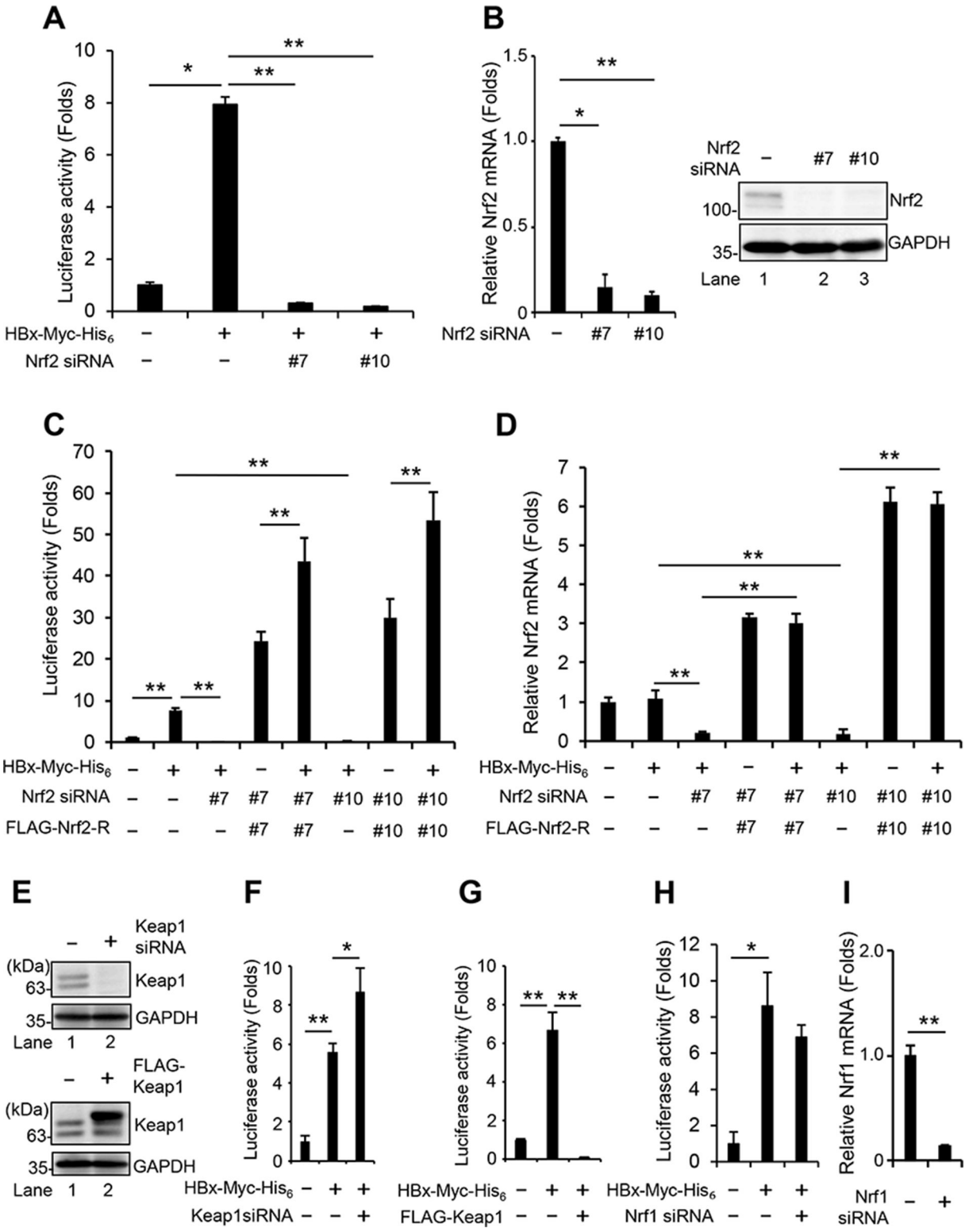

FIG 2 Nrf2 is involved in the HBx-induced antioxidant response. HepG2 cells were transfected with 40 nM Nrf2 siRNA #7, Nrf2 siRNA #10, or control siRNA. At 24 h after siRNA transfection, the cells were co-transfected with pGL4.37[luc2P/ARE/Hygro] and pEF1A-HBx-Myc-His$_6$ (A and B), or together with one of the siRNA-resistant plasmids pCAG-FLAG-Nrf2-R #7 or pCAG-FLAG-Nrf2-R #10 (C and D). At 48 h after plasmid transfection, the cells were harvested. ARE-luciferase activity was measured and normalized to *Renilla* activity (A and C). The mRNA levels of Nrf2 were quantitated by real-time RT-PCR (B, left panel and D). The expression levels of endogenous Nrf2 protein in cell lysates were analyzed by immunoblotting with anti-Nrf2 monoclonal antibody (MAb) (B, right panel). The

(Continued on next page)

FIG 2 (Continued)

level of glyceraldehyde-3-phosphate dehydrogenase (GAPDH) served as a loading control. (E, F, and G) HepG2 cells were transfected with 40 nM Keap1 siRNA or pCAG-FLAG-Keap1, together with pGL4.37[luc2P/ARE/Hygro] and pEF1A-HBx-Myc-His_6. At 48 h after plasmid transfection, the expression of Keap1 in cell lysates was analyzed by immunoblotting with anti-Keap MAb (E, top and third panels). The level of GAPDH served as a loading control (E). ARE-luciferase activity was measured and normalized to *Renilla* activity (F and G). (H and I) HepG2 cells were transfected with 40 nM nuclear factor erythroid 2-related factor 1 (Nrf1) siRNA or control siRNA. At 24 h after siRNA transfection, the cells were co-transfected with pGL4.37[luc2P/ARE/Hygro] and pEF1A-HBx-Myc-His_6. At 48 h after plasmid transfection, ARE-luciferase activity was measured and normalized to *Renilla* activity (H). The mRNA levels of Nrf1 were quantitated by real-time RT-PCR (I). The data represent the means ± SEM of data from three independent experiments, and the value for the control cells was arbitrarily expressed as 1.0. *$P < 0.05$, **$P < 0.01$.

the presence or absence of Nrf2 small interfering RNAs (siRNAs) #7 and #10, respectively. Knockdown of Nrf2 markedly decreased HBx-induced ARE-luciferase activity (Fig. 2A), when endogenous Nrf2 mRNA and Nrf2 protein were significantly knocked down by Nrf2 siRNAs #7 and #10 (Fig. 2B). To determine whether the ARE-luciferase activity resulting from depletion of Nrf2 is recovered by addition of siRNA-resistant Nrf2, we transfected the plasmid encoding FLAG-tagged siRNA-resistant Nrf2 (FLAG-Nrf2-R #7 or FLAG-Nrf2-R #10). Overexpression of the FLAG-Nrf2-R #7 or FLAG-Nrf2-R #10 significantly increased the ARE-luciferase activity (Fig. 2C), when Nrf2 mRNA levels were recovered by transfection of the FLAG-Nrf2-R #7 or FLAG-Nrf2-R #10 plasmid (Fig. 2D). Notably, HBx still promoted FLAG-Nrf2-R #7- or FLAG-Nrf2-R #10-induced ARE-luciferase activity (Fig. 2C). These results suggest that Nrf2 is involved in the HBx-induced antioxidant response.

To further validate the effect of Nrf2 on the HBx-induced antioxidant response, we investigated the impact of Keap1, a negative regulator of Nrf2, on the HBx-induced antioxidant response. HepG2 cells were transfected with Keap1 siRNA or pCAG-FLAG-Keap1, together with pEF1A-HBx-Myc-His6 and pGL4.37[luc2P/ARE/Hygro]. Keap1 protein level was markedly reduced by Keap1 siRNA (Fig. 2E, top panel, lane 2), and conversely, Keap1 protein level was increased via overexpression of Keap1 (Fig. 2E, third panel, lane 2). The luciferase assay demonstrated a significant increase in HBx-induced ARE-luciferase activity upon Keap1 knockdown (Fig. 2F). Conversely, the overexpression of Keap1 led to a notable reduction in HBx-induced ARE-luciferase activity (Fig. 2G). These results suggest that Keap1 suppresses the HBx-induced antioxidant response by inhibiting Nrf2 activity.

Like Nrf2, the transcription factor nuclear factor erythroid 2-related factor 1 (Nrf1) belongs to the Cap-N-Collar family. To determine whether Nrf1 is also involved in the HBx-induced ARE-luciferase activity, HepG2 cells were co-transfected with pEF1A-HBx-Myc-His_6 and pGL4.37[luc2P/ARE/Hygro] in the presence or absence of Nrf1 siRNA. Knockdown of Nrf1 did not show any significant effect on the HBx-induced ARE-luciferase activity (Fig. 2H), when endogenous Nrf1 mRNA expression was significantly reduced by Nrf1 siRNA (Fig. 2I). These results suggest that Nrf2 is specifically involved in the HBx-induced antioxidant response.

HBx upregulates Nrf2 protein levels

To clarify the relationship between Nrf2 activation and the HBV life cycle, we first examined the effects of HBV infection on Nrf2 abundance at the protein and mRNA levels by immunoblot and real-time RT-PCR analyses, respectively. The endogenous Nrf2 protein level was increased in HBV-infected HepG2-hNTCP-C4 cells at 12 dpi compared to that in the mock-infected cells (Fig. 3A, upper panel). Notably, HBV infection did not show any significant effect on the Nrf2 mRNA level (Fig. 3A, bottom panel). These results suggest that HBV infection upregulates the endogenous Nrf2 protein level but not the Nrf2 mRNA level.

To determine which HBV protein is involved in HBV-induced upregulation of Nrf2 protein, HepG2 cells were transfected with either pEF1A-HBx-Myc-His_6 or pEF1A-HBc-Myc-His_6. The immunoblot analysis showed that the endogenous Nrf2 protein level was increased in HBx-expressing cells (Fig. 3B, upper panel) but not in HBc-expressing cells

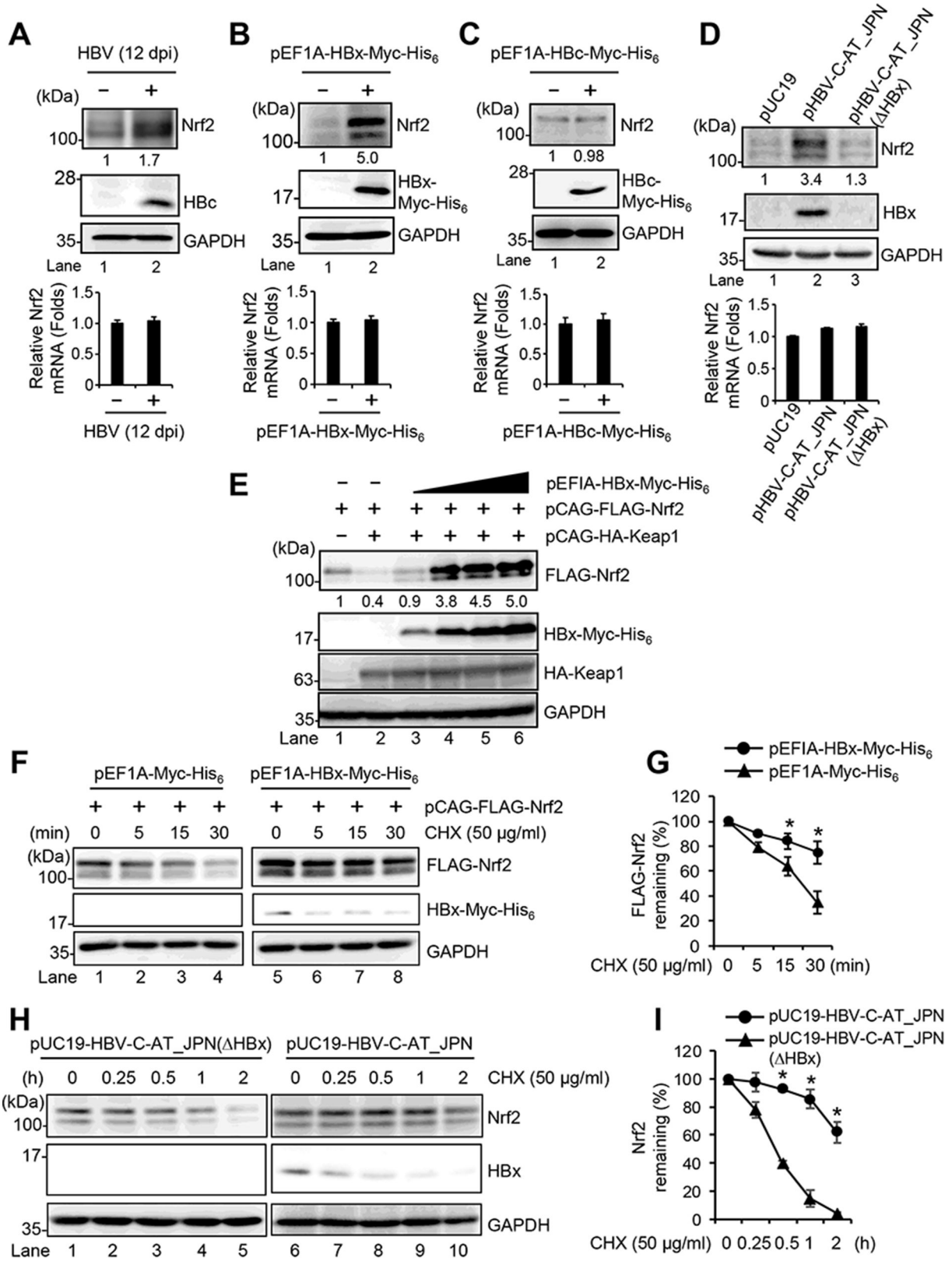

FIG 3 HBx upregulates Nrf2 protein levels. (A) HepG2-hNTCP-C4 cells were infected with HBV at 40,000 genome equivalents/cell. The cells were harvested at 12 dpi. HepG2 cells were transfected with pEF1A-HBx-Myc-His$_6$ (B), pEF1A-HBc-Myc-His$_6$ (C), or pUC19-HBV-C-AT_JPN or pUC19-HBV-C-AT_JPN(ΔHBx) (D), followed by incubation for 48 h. The expression levels of endogenous Nrf2 protein in cell lysates were analyzed by immunoblotting with anti-Nrf2 monoclonal

(Continued on next page)

FIG 3 (Continued)

antibody (MAb) (A, B, C, and D, top panels). The relative expression levels of endogenous Nrf2 were quantified by densitometry and indicated below in the respective lanes. The expression levels of HBc in HBV-infected HepG2-hNTCP-C4 cells and of Myc-His_6-tagged HBx, Myc-His_6-tagged HBc, and HBx in pUC19-HBV-C-AT_JPN-transfected cells were analyzed by immunoblotting with anti-HBc MAb (A, second panel), anti-c-Myc MAb (B and C, second panels), and anti-HBx polyclonal antibody (PAb) (D, second panel), respectively. The level of glyceraldehyde-3-phosphate dehydrogenase (GAPDH) served as a loading control. Nrf2 mRNA levels were analyzed by real-time RT-PCR (A, B, C, and D, bottom panels). (E) HepG2 cells were co-transfected with pCAG-FLAG-Nrf2 and pCAG-HA-Keap1 together with increasing amounts of pEF1A-HBx-Myc-His_6. At 48 h after transfection, the cells were harvested, and cell lysates were analyzed by immunoblotting with anti-Nrf2 MAb (first panel), anti-c-Myc MAb (second panel), anti-HA PAb (third panel), and anti-GAPDH MAb (fourth panel), respectively. The relative expression levels of FLAG-Nrf2 were quantitated by densitometry and indicated below in the respective lanes. The level of GAPDH served as a loading control. (F) HepG2 cells were transfected with pCAG-FLAG-Nrf2 together with either pEF1A-HBx-Myc-His_6 or pEF1A-Myc-His_6. At 40 h after transfection, cells were treated with a reversible inhibitor of proteasomes, MG132, at 25 µM and cultured for 8 h. Before cycloheximide (CHX) addition, MG132 was washed away with fresh medium. Then, the cells were treated with 50 µg/mL CHX at 48 h after transfection. The cell lysates were harvested at 0, 5, 15, and 30 min after treatment with CHX, followed by immunoblotting with anti-Nrf2 MAb (top panel), anti-c-Myc MAb (middle panel), and anti-GAPDH MAb (bottom panel). The level of GAPDH served as a loading control. (G) Specific signals were quantitated by densitometry, and the percentage of remaining FLAG-Nrf2 at each time point was compared with that at time point zero. Closed triangles, pEF1A-Myc-His_6; closed circles, pEF1A-HBx-Myc-His_6. The data represent the means ± SEM of data from three independent experiments. *P < 0.05 compared with the controls. (H) HepG2 cells were transfected with pUC19-HBV-C-AT_JPN or pUC19-HBV-C-AT_JPN(ΔHBx). At 40 h after transfection, 25 µM MG132 was added to the cells for an 8-h treatment. The cells were then treated with 50 µg/mL CHX at 48 h after transfection. The cell lysates were harvested at 0, 0.25, 0.5, 1, and 2 h after treatment with CHX, followed by immunoblotting with anti-Nrf2 MAb (top panel), anti-HBx PAb (middle panel), and anti-GAPDH MAb (bottom panel). The level of GAPDH served as a loading control. (I) Specific signals were quantitated by densitometry, and the percentage of remaining endogenous Nrf2 at each time point was compared with that at time point zero. Closed triangles, pUC19-HBV-C-AT_JPN(ΔHBx); closed circles, pUC19-HBV-C-AT_JPN. The data represent the means ± SEM of data from three independent experiments. *P < 0.05 compared with the controls.

(Fig. 3C, upper panel). Neither HBx nor HBc had any effect on the levels of Nrf2 mRNA expression (Fig. 3B, bottom panel; Fig. 3C, bottom panel). To further verify the role of HBx in HBV-induced upregulation of the Nrf2 protein, HepG2 cells were transfected with either pUC19-HBV-C-AT_JPN or pUC19-HBV-C-AT_JPN(ΔHBx). The immunoblot analysis showed that the endogenous Nrf2 protein level was increased in HBV-C-AT_JPN-replicating cells but not in HBV-C-AT_JPN (ΔHBx)-replicating cells (Fig. 3D, upper panel, lanes 2 and 3). Similarly, HBV replication did not show any effect on endogenous Nrf2 mRNA expression in either the presence or absence of HBx protein (Fig. 3D, bottom panel). This result suggests that HBx is involved in HBV-induced upregulation of the endogenous Nrf2 protein level but not the Nrf2 mRNA level.

To further examine the effect of HBx on the Nrf2 protein levels, HepG2 cells were co-transfected with pCAG-FLAG-Nrf2, pCAG-HA-Keap1, and pEF1A-HBx-Myc-His_6. The amount of FLAG-Nrf2 protein was decreased in pCAG-HA-Keap1-transfected cells (Fig. 3E, first panel, lanes 1 and 2). However, FLAG-Nrf2 protein levels increased depending on the amount of HBx plasmids (Fig. 3E, first panel, lanes 3–6), suggesting that HBx upregulates the Nrf2 protein level.

To determine whether HBx-induced upregulation of Nrf2 protein is due to a decrease in the rate of Nrf2-degradation, we performed kinetic analysis using the protein synthesis inhibitor cycloheximide (CHX). A FLAG-Nrf2 protein plasmid together with an HBx-Myc-His_6 plasmid or control plasmid was transfected into HepG2 cells. Cells were collected at 0, 5, 15, and 30 min following treatment with 50 µg/mL CHX and analyzed by immunoblotting (Fig. 3F). The CHX-chase analysis revealed that overexpression of HBx resulted in slow degradation of the FLAG-Nrf2 protein compared to the control (Fig. 3G), suggesting that HBx enhances Nrf2 protein stability. To further verify the effect of HBx on endogenous Nrf2 protein stability, HepG2 cells were transfected with either pUC19-HBV-C-AT_JPN or pUC19-HBV-C-AT_JPN(ΔHBx). Cells were collected at 0, 0.25, 0.5, 1, and 2 h after treatment with CHX and analyzed by immunoblotting (Fig. 3H). Similarly, the CHX-chase analysis revealed that HBV enhanced the stability of endogenous Nrf2 protein compared to HBx-deficient HBV (Fig. 3I). These results indicate that HBx enhances Nrf2 stability.

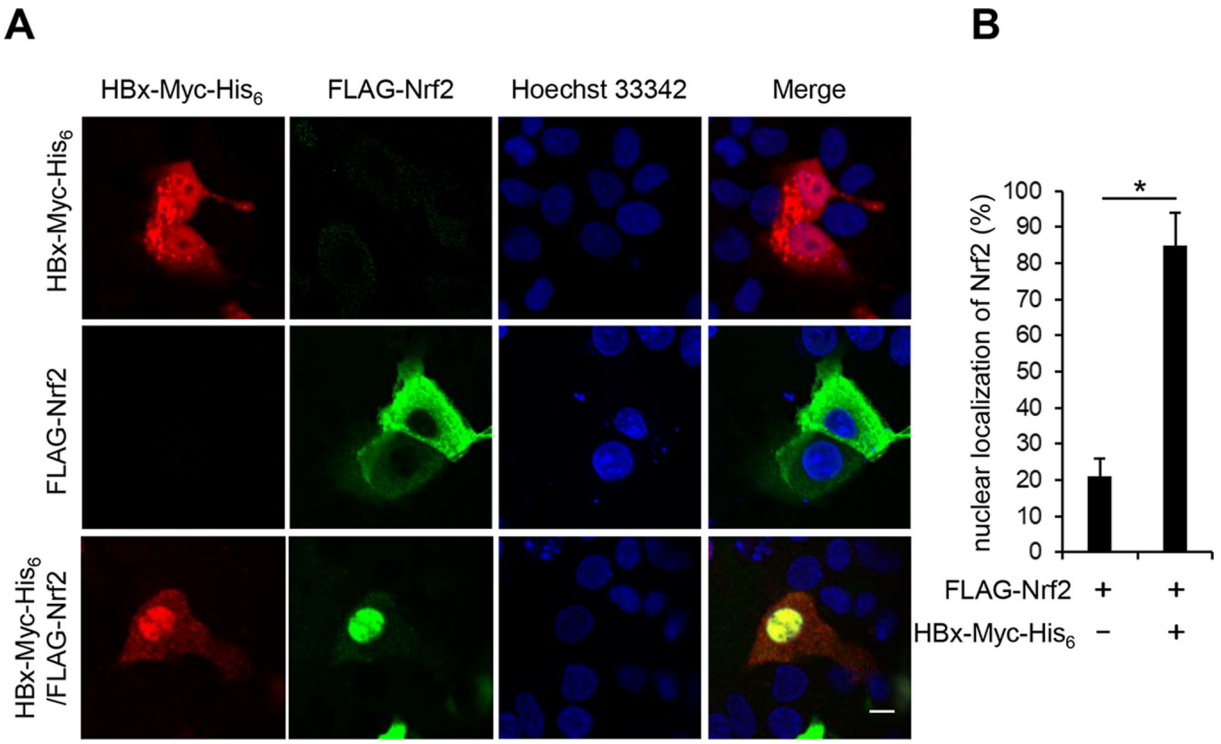

FIG 4 HBx induces Nrf2 nuclear localization. (A) HepG2 cells were transfected with pEF1A-HBx-Myc-His$_6$ (top panel), pCAG-FLAG-Nrf2 (middle panel), or pEF1A-HBx-Myc-His$_6$ plus pCAG-FLAG-Nrf2 (bottom panel). At 48 h after transfection, the cells were stained with anti-c-Myc mouse monoclonal antibody, followed by Alexa Fluor 594-conjugated goat anti-mouse IgG (red) and anti-FLAG rabbit polyclonal antibody, followed by Alexa Fluor 488-conjugated goat anti-rabbit IgG (green). The cell nuclei were stained with Hoechst 33342 (blue). Scale bar, 5 µm. (B) The percentage of cells with FLAG-Nrf2 nuclear localization was determined for HBx-Myc-His$_6$-expressing cells and control cells. The data represent the means ± SEM of data from three independent experiments. *$P < 0.05$.

HBx induces Nrf2 nuclear localization

To determine the effect of HBx on Nrf2 subcellular localization, we performed indirect immunofluorescence staining. HepG2 cells were transfected with the plasmid pEF1A-HBx-Myc-His$_6$, the plasmid pCAG-FLAG-Nrf2, or both. When pEF1A-HBx-Myc-His$_6$ alone was transfected, the HBx-Myc-His$_6$ protein was localized in both the nucleus and the cytoplasm (Fig. 4A, top panel). FLAG-Nrf2 was mainly localized in the cytoplasm (Fig. 4A, second panel). When pEF1A-HBx-Myc-His$_6$ and pCAG-FLAG-Nrf2 were co-transfected into the cells, FLAG-Nrf2 was predominantly localized in the nucleus (Fig. 4A, third panel, Merge). FLAG-Nrf2 was localized in the nucleus in approximately 85% of HBx-Myc-His$_6$-expressing cells (Fig. 4B). These results suggest that HBx induces Nrf2 nuclear localization, leading to Nrf2 activation. Although we examined the localization of endogenous Nrf2 protein, we failed to detect endogenous Nrf2, probably due to the lack of an appropriate anti-Nrf2 antibody for immunofluorescence staining.

Nrf2 is involved in the suppression of intracellular HBV RNA and pregenomic RNA

To determine the effects of Nrf2 activation on HBV replication, HepG2 cells were transfected with either pCAG-FLAG-Nrf2 or Nrf2 siRNA together with expression plasmids containing HBV genotypes A, B, C, and D: pUC19-HBV-AeuS, pUC19-HBV-Bj_JPN56, pUC19-HBV-C-AT_JPN, or pUC19-HBV-D-IND60, respectively. HBV transcripts were then quantified by real-time RT-PCR using primers for amplification of the HBV RNA, including pregenomic RNA (pgRNA) and 2.4/2.1 kb HBsAg mRNA, or HBV pgRNA only. Overexpression of Nrf2 markedly decreased the intracellular HBV RNA and pgRNA levels of HBV-AeuS (Fig. 5A), HBV-Bj_JPN56 (Fig. 5B), HBV-C-AT_JPN (Fig. 5C), and

pHBV-D-IND60 (Fig. 5D) compared to the controls. Conversely, knockdown of endogenous Nrf2 significantly increased the intracellular HBV RNA and pgRNA levels of HBV-AeuS (Fig. 5E), HBV-Bj_JPN56 (Fig. 5F), HBV-C-AT_JPN (Fig. 5G), and pHBV-D-IND60 (Fig. 5H) compared to the controls. These results suggest that Nrf2 is involved in the suppression of HBV replication.

Nrf2 is involved in the suppression of intracellular HBc and HBs protein levels as well as extracellular HBeAg and HBsAg levels

To examine the roles of Nrf2 in the intracellular HBc and HBs protein levels as well as the extracellular HBeAg and HBsA levels, HepG2 cells were transfected with either pCAG-FLAG-Nrf2 or Nrf2 siRNA together with HBV plasmids pUC19-HBV-AeuS, pUC19-HBV-Bj_JPN56, pUC19-HBV-C-AT_JPN, or pUC19-HBV-D-IND60. The immunoblot analysis revealed that overexpression of Nrf2 markedly decreased the HBc protein levels (Fig. 6A, top panel, lanes 2, 4, 6, and 8) and moderately decreased the HBs levels (Fig. 6A, second panel, lanes 2, 4, 6, and 8) in HBV-AeuS, HBV-Bj_JPN56, HBV-C-AT_JPN, or HBV-D-IND60-replicating cells. Notably, the inhibitory effect of Nrf2 overexpression on HBs levels appeared to be genotype-dependent, strongly inhibiting the HBs of genotypes C-AT_JPN and D-IND60 (Fig. 6A, second panel, lanes 6 and 8), whereas only slightly inhibiting the HBs of genotypes AeuS and Bj_JPN56 (Fig. 6A, second panel, lanes 2 and 4). However, overexpression of Nrf2 did not decrease intracellular HBx protein levels (Fig. 6A, third panel, lanes 2, 4, 6, and 8), suggesting that Nrf2 does not affect HBx mRNA transcription. It is noteworthy that overexpression of Nrf2 slightly increased the levels of HBx in genotypes AeuS and D-IND60 (Fig. 6A, third panel, lanes 2 and 8), which is consistent with the notion that the effect of Nrf2 on HBx levels is genotype-dependent.

Consistent with the above results, an ELISA assay showed that overexpression of Nrf2 significantly decreased the amount of extracellular HBeAg (Fig. 6B) and HBsAg (Fig. 6C) in HBV-AeuS-, HBV-Bj_JPN56-, HBV-C-AT_JPN-, or HBV-D-IND60-replicating cells. Conversely, knockdown of endogenous Nrf2 significantly increased the amount of extracellular HBeAg (Fig. 6D) and HBsAg (Fig. 6E) in these HBV-replicating cells. These results suggest that Nrf2 decreases the amounts of intracellular HBc and HBs protein expression as well as the levels of extracellular HBeAg and HBsAg.

To further assess the role of Nrf2 in HBV propagation in HBV-infected cells, HBV-infected HepG2-hNTCP-C4 cells were transfected with either pCAG-FLAG-Nrf2 or Nrf2 siRNA. The intracellular HBV RNA and pgRNA levels at 4 dpi were determined by real-time RT-PCR. Overexpression of Nrf2 strongly increased the Nrf2 mRNA level (Fig. 7A, right panel), which in turn significantly decreased the amounts of intracellular HBV RNA and pgRNA (Fig. 7A, left and middle panels). Conversely, knockdown of Nrf2 significantly decreased the levels of Nrf2 mRNA (Fig. 7B, third panel) and Nrf2 protein (Fig. 7B, fourth panel), resulting in a significant increase in the amounts of intracellular HBV RNA and pgRNA (Fig. 7B, first and second panels). On the other hand, overexpression of Nrf2 also significantly decreased extracellular HBeAg (Fig. 7C, left panel) and HBsAg (Fig. 7D, left panel), whereas knockdown of Nrf2 significantly increased extracellular HBeAg (Fig. 7C, right panel) and HBsAg (Fig. 7D, right panel). These results suggest that Nrf2 plays a role in inhibiting HBV propagation.

Nrf2 strongly suppresses HBV core promoter activity

Next, to determine whether Nrf2-mediated inhibition of HBV RNA is due to a transcriptional mechanism, we examined the effects of overexpression or knockdown of Nrf2 on the activities of four different HBV promoters [core, preS1, preS2/S, and enhancer 1 (Enh1)/X] derived from HBV genotype Ce. HepG2 cells were co-transfected with either pCAG-FLAG-Nrf2 or Nrf2 siRNA together with the firefly luciferase reporter driven by the core, preS1, preS2/S, or Enh1/X promoters, respectively. The promoter reporter assays demonstrated that overexpression of Nrf2 markedly reduced the HBV core promoter activity (Fig. 8A) and significantly reduced HBV preS1 promoter activity (Fig. 8B) and preS2/S (Fig. 8C) promoter activity. Overexpression of Nrf2 did not show any significant

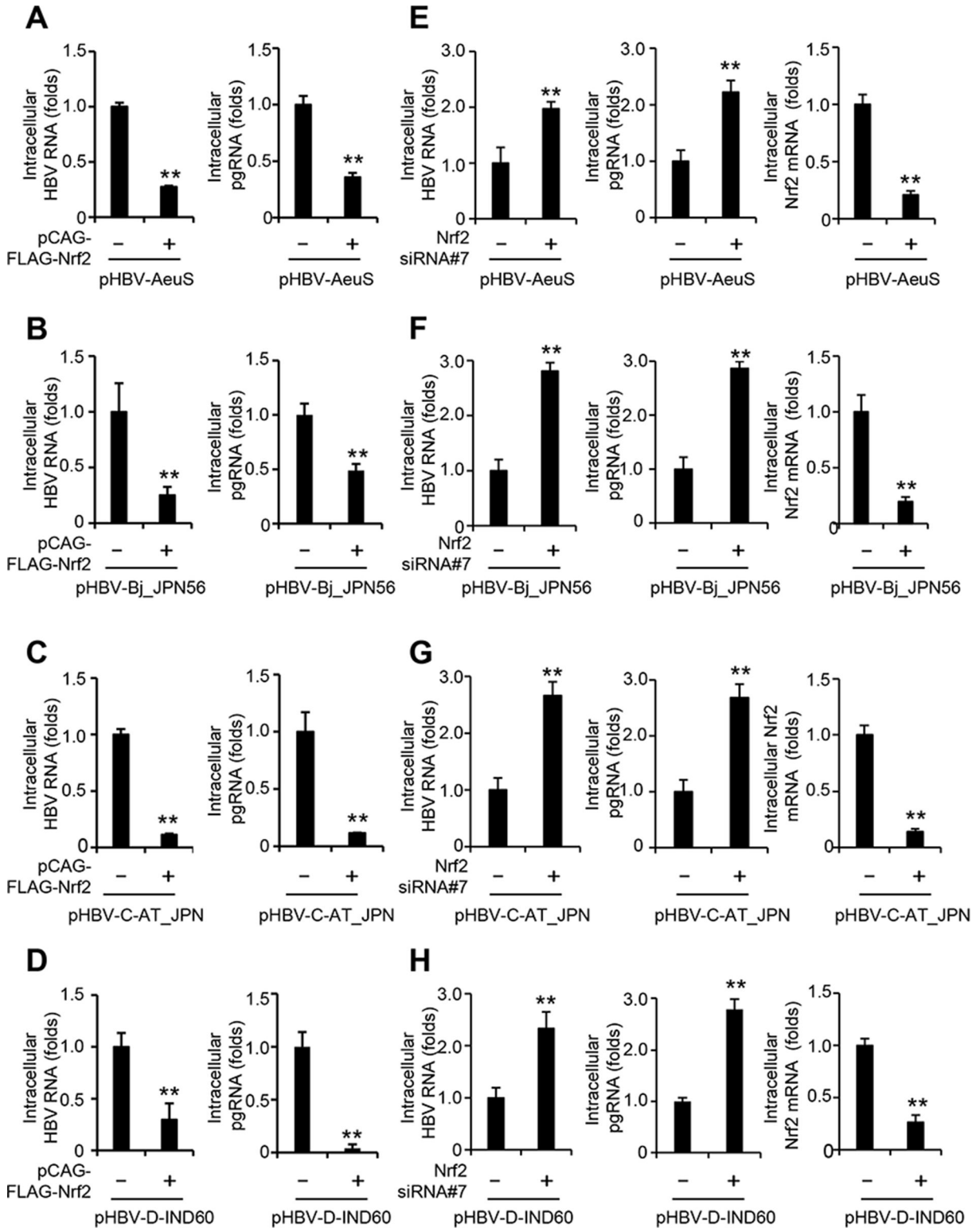

FIG 5 Nrf2 is involved in the suppression of intracellular HBV RNA and pgRNA. HepG2 cells were transfected with pCAG-FLAG-Nrf2 or 40 nM Nrf2 siRNA #7, together with one of four HBV expression plasmids carrying a 1.3-mer overlength HBV genome: pUC19-HBV-AeuS (A and E), pUC19-HBV-Bj_JPN56 (B and F), pUC19-HBV-C-AT_JPN (C and G), or pUC19-HBV-D-IND60 (D and H). Total RNA was extracted 48 h after transfection. The amounts of HBV RNA and pgRNA were quantitated by real-time RT-PCR. The data represent the means ± SEM of data from three independent experiments, and the value for the control cells was arbitrarily expressed as 1.0. $^{**}P < 0.01$ compared with the controls.

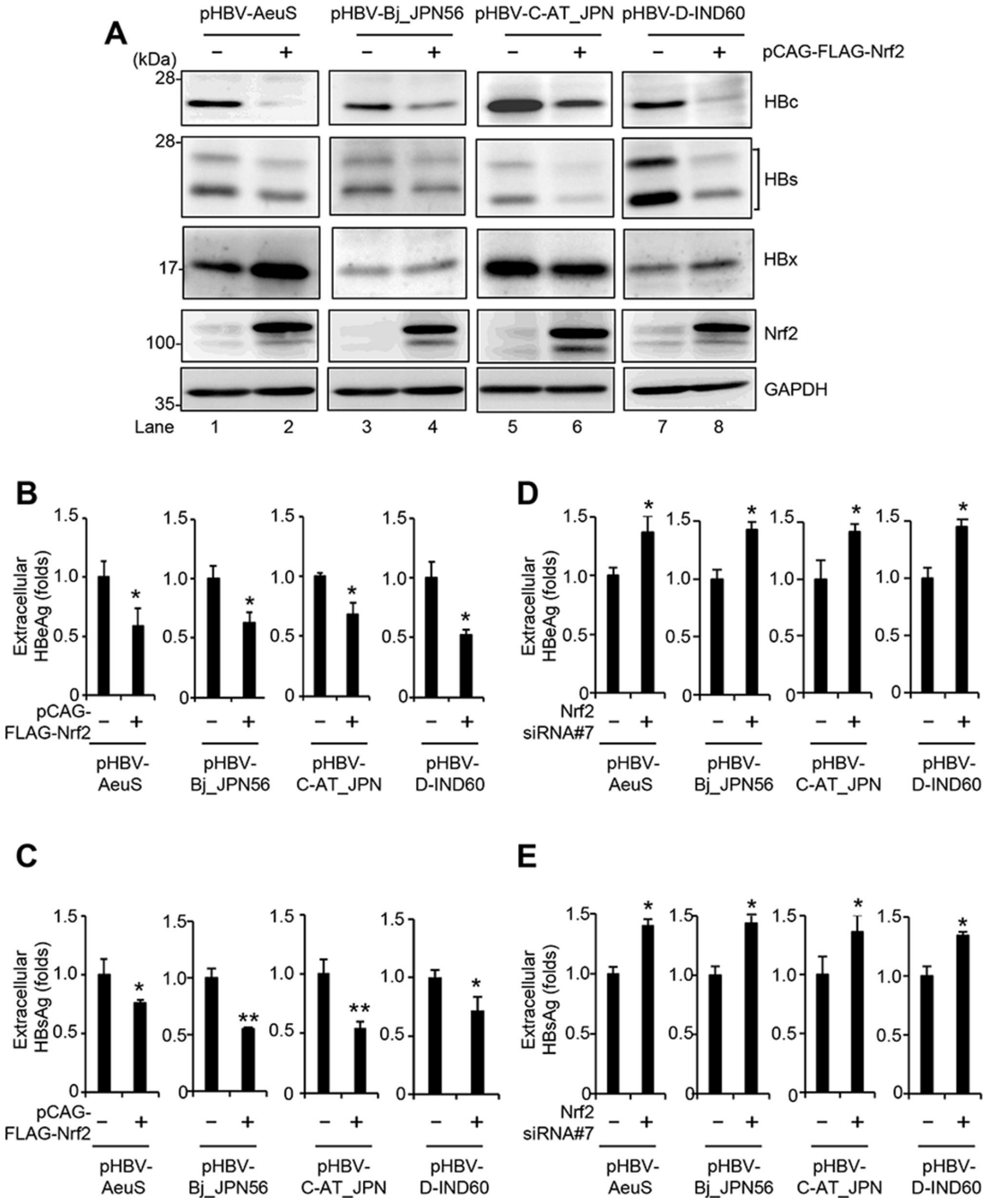

FIG 6 Nrf2 is involved in the suppression of intracellular HBc and HBs protein levels as well as extracellular HBeAg and HBsAg levels. (A, B, and C) HepG2 cells were transfected with pCAG-FLAG-Nrf2 together with an HBV expression plasmid that carries the 1.3-mer overlength HBV genome, pUC19-HBV-AeuS, pUC19-HBV-Bj_JPN56, pUC19-HBV-C-AT_JPN, or pUC19-HBV-D-IND60, followed by incubation for 48 h. The expression levels of HBc, HBs, HBx, Nrf2, and glyceraldehyde-3-phosphate dehydrogenase (GAPDH) in FLAG-Nrf2-expressing cell lysate were analyzed by immunoblotting with anti-HBc monoclonal antibody (MAb) (first panel), anti-HBs polyclonal antibody (PAb) (second panel), anti-HBx PAb (third panel), anti-Nrf2 MAb (fourth panel), and anti-GAPDH MAb (fifth panel), respectively. The level of GAPDH served as a loading control. (D and E) HepG2 cells were transfected with 40 nM Nrf2 siRNA #7 together with an HBV expression plasmid that carries the 1.3-mer overlength HBV genome, pUC19-HBV-AeuS, pUC19-HBV-Bj_JPN56, pUC19-HBV-C-AT_JPN, or pUC19-HBV-D-IND60, followed by incubation for 48 h. The levels of HBeAg (B and D) and HBsAg (C and E) in the culture supernatant of HBV-AeuS, HBV-Bj_JPN56, HBV-C-AT_JPN, or HBV-D-IND60-replicating cells were measured by ELISA. The data represent the means ± SEM of data from three independent experiments, and the value for the control cells was arbitrarily expressed as 1.0. *$P < 0.05$, **$P < 0.01$, compared with the controls.

effect on the Enh1/X promoter activity (Fig. 8D). Conversely, knockdown of Nrf2 significantly increased the activities of the HBV core promoter (Fig. 8E), preS1 promoter (Fig. 8F), and preS2/S promoter (Fig. 8G). Knockdown of Nrf2 showed no significant effect on Enh1/X promoter activity (Fig. 8H). These results are consistent with the notion that Nrf2 does not affect HBx mRNA transcription.

To further verify the inhibitory effect of Nrf2 on HBV core promoter activity, we analyzed the impact of Nrf2 on HBV core promoters derived from HBV genotypes Aa, Bj, and D using the firefly luciferase reporter systems. Promoter reporter assays showed that overexpression of Nrf2 strongly reduced the activities of the HBV core promoters derived from HBV genotypes Aa, Bj, or D (Fig. 8I). Conversely, knockdown of endogenous Nrf2 significantly enhanced the activities of these HBV core promoters (Fig. 8J). We confirmed that endogenous Nrf2 was efficiently knocked down by siRNA (Fig. 8K). These results suggest that Nrf2 strongly suppresses HBV core promoter activity, leading to a decrease in the amounts of intracellular HBV pgRNA/precore mRNA, HBc protein, and extracellular HBeAg.

Nrf2 binds to the HBV core promoter

To determine whether the HBV core promoter has a putative Nrf2-binding site, we analyzed the HBV genotype Ce core promoter (GenBank accession number AB014381) using the JASPAR 2022 database of transcription factor binding sites. A putative Nrf2-binding motif was found within the HBV Ce core promoter from nucleotides (nt) 1,667 to 1,679, 5′-TGGACTCTCAGCA-3′ (Fig. 9A). To assess whether Nrf2 interacts with the HBV core promoter, chromatin immunoprecipitation and quantitative PCR (ChIP-qPCR) were performed. The results showed that the level of HBV DNA was significantly higher in the FLAG-Nrf2 immunoprecipitate than in the control (Fig. 9B). The amount of FLAG-Nrf2 immunoprecipitate was confirmed by immunoblotting (Fig. 9C, upper panel, lane 4). These results suggest that Nrf2 binds to the HBV core promoter.

To identify the specific sites in the HBV core promoter required for the interaction with Nrf2, we introduced a double-point mutation (G1669C/A1670T) into the HBV Ce core promoter, which is highly conserved in the predicted Nrf2-binding motif (Fig. 9A). The ChIP-qPCR analysis revealed that the double-point mutant HBV Ce core promoter G1669C/A1670T significantly reduced the interaction with Nrf2 (Fig. 9D). On the other hand, the double-point mutant HBV Ce core promoter A1676C/C1678A (Fig. 9A) did not affect the interaction between Nrf2 and the HBV Ce core promoter (Fig. 9D). These results suggest that the HBV Ce core promoter from nt 1,667 to 1,679 is involved in the interaction between Nrf2 and the HBV core promoter.

HBx-mediated ROS production is not involved in HBx-induced ARE-luciferase activity

To investigate whether HBx-induced ROS production is involved in HBx-induced ARE-luciferase activity, we treated the HBx-Myc-His_6-expessing cells with the antioxidant *N*-acetyl cysteine (NAC), which is a scavenger of ROS. To examine the ROS production in HBx-Myc-His_6-expressing cells, we performed immunofluorescence staining by using MitoSOX, a fluorescent probe specific for mitochondrial superoxide. HBx-Myc-His_6-expressing cells displayed much stronger red signals than the control. Treatment with NAC clearly reduced HBx-induced mitochondrial ROS production (Fig. 10A, second panel, MitoSOX). However, the ARE-luciferase reporter assay showed that NAC treatment did not show any significant effect on HBx-induced ARE-luciferase activity (Fig. 10B). The immunoblot analysis also showed that NAC treatment did not have any significant effect on endogenous Nrf2 protein levels in HepG2 cells transfected with pEF1A-HBx-Myc-His_6 (Fig. 10C). These results suggest that HBx-mediated ROS production is not involved in HBx-induced ARE-luciferase activity.

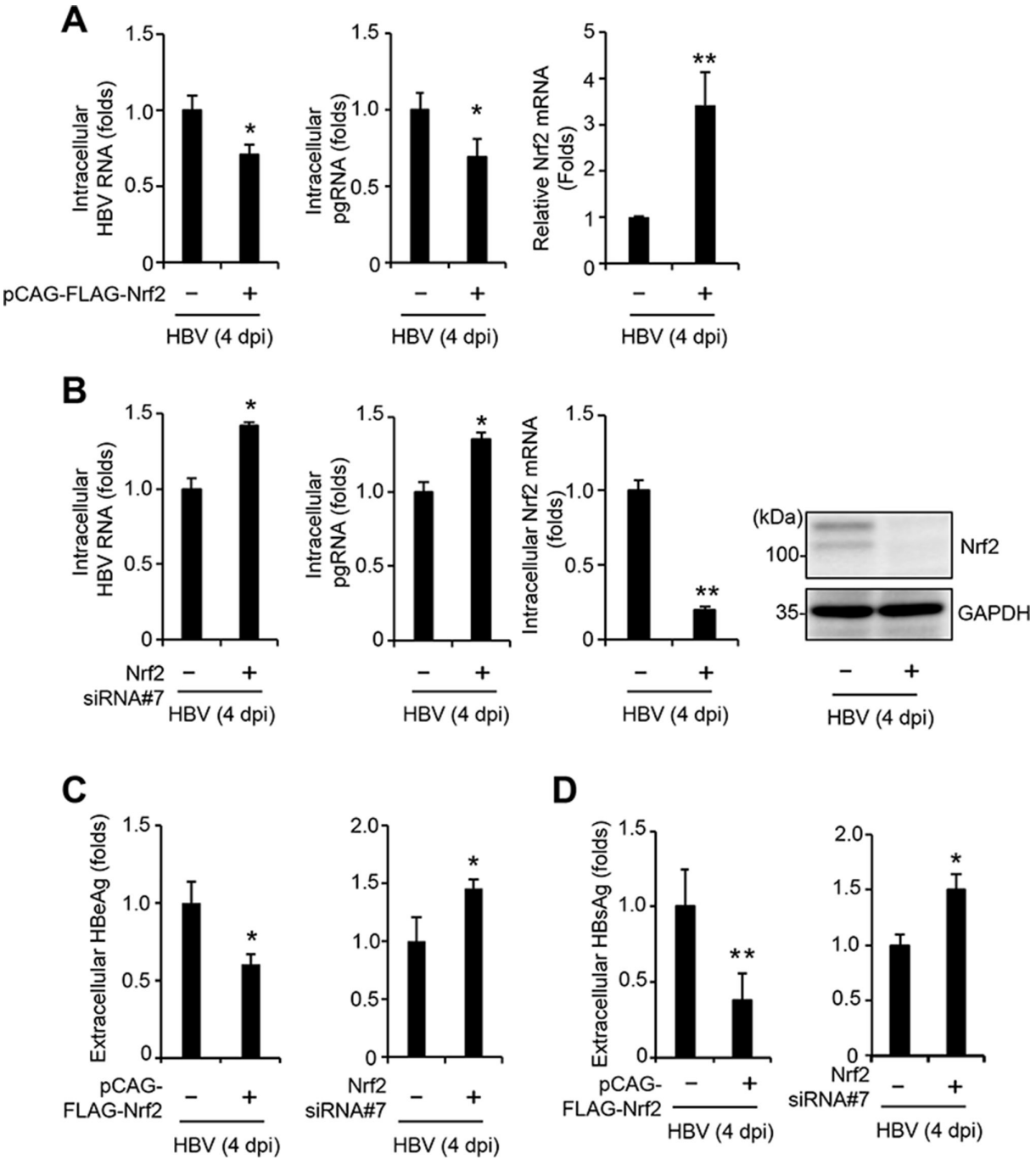

FIG 7 Nrf2 significantly decreases the amounts of intracellular HBV RNA and pgRNA as well as extracellular HBeAg and HBsAg in HBV-infected HepG2-hNTCP-C4 cells. HepG2-hNTCP-C4 cells were infected with HBV at 40,000 genome equivalents/cell. At 24 h after inoculation, the cells were transfected with pCAG-FLAG-Nrf2 or 40 nM Nrf2 siRNA #7, followed by incubation for 4 days. Total RNA was extracted, and the amounts of intracellular HBV RNA, pgRNA, and Nrf2 mRNA (A and B) were quantitated by real-time RT-PCR. The expression levels of endogenous Nrf2 protein in Nrf2 siRNA-transfected cell lysate were analyzed by immunoblotting using anti-Nrf2 monoclonal antibody (B, fourth panel). The level of glyceraldehyde-3-phosphate dehydrogenase (GAPDH) served as a loading control. The levels of HBeAg (C) and HBsAg (D) in the culture supernatant of HBV-infected HepG2-hNTCP-C4 cells were measured by ELISA. The data represent the means ± SEM of data from three independent experiments, and the value for the control cells was arbitrarily expressed as 1.0. *$P < 0.05$, **$P < 0.01$, compared with the controls.

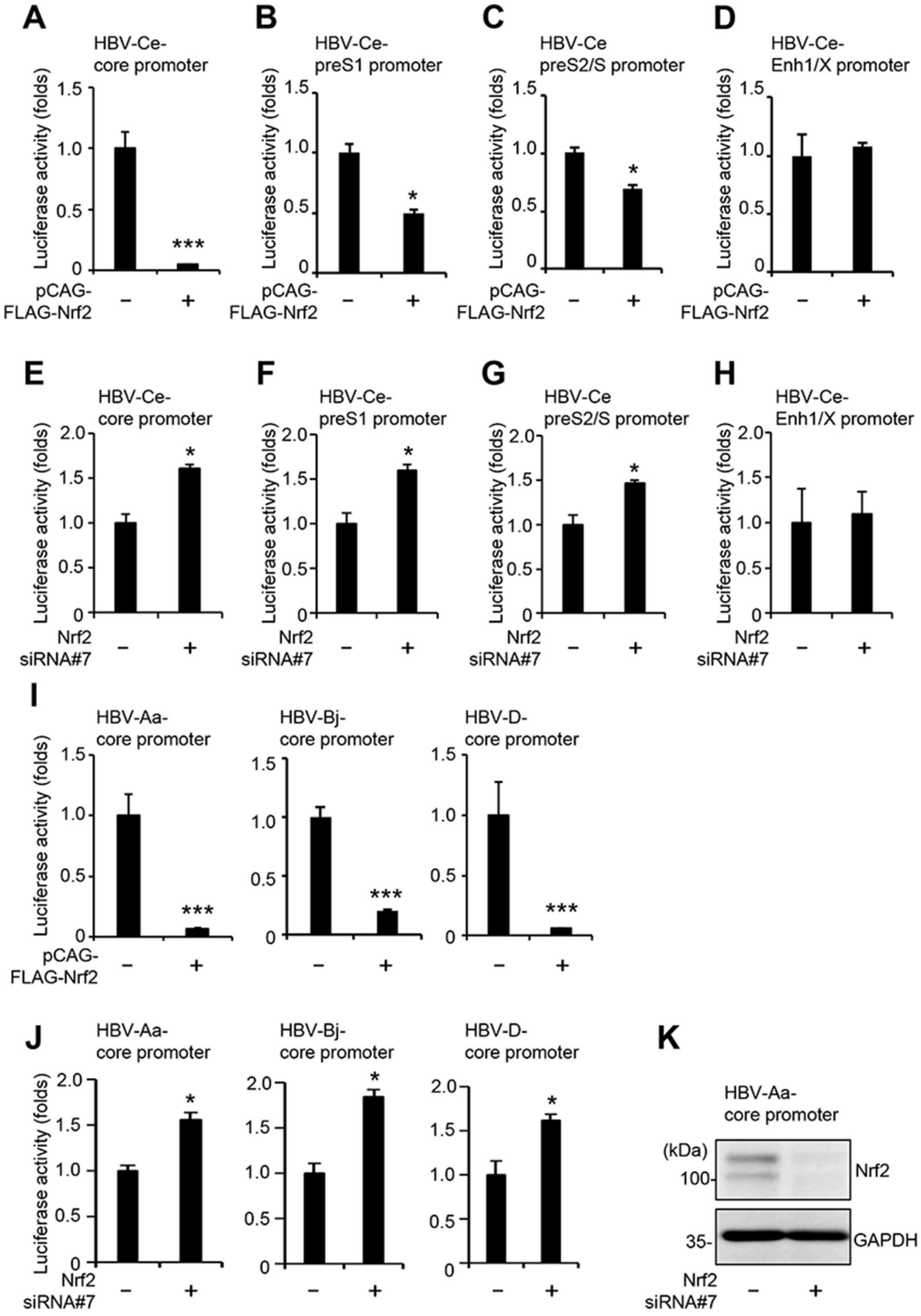

FIG 8 Nrf2 strongly suppresses HBV core promoter activity. HepG2 cells were transfected with pCAG-FLAG-Nrf2 or 40 nM Nrf2 siRNA #7 together with the firefly luciferase reporter plasmid driven by the entire HBV Ce core promoter (A and E), HBV Ce preS1 promoter (B and F), HBV Ce preS2/S promoter (C and G), HBV Ce Enh1/X promoter (D and H), or entire HBV core promoters from genotypes Aa, Bj, or D (I and J). At 48 h after transfection, the expression levels

(Continued on next page)

FIG 8 (Continued)

of endogenous Nrf2 protein in Nrf2 siRNA-transfected cell lysates were analyzed by immunoblotting using anti-Nrf2 monoclonal antibody (K). The level of glyceraldehyde-3-phosphate dehydrogenase (GAPDH) served as a loading control. The luciferase activity was measured and normalized to *Renilla* activity. The data represent the means ± SEM of data from three independent experiments, and the value for the control cells was arbitrarily expressed as 1.0. $*P < 0.05$, $***P < 0.001$, compared with the controls.

HBx does not affect the half-life of endogenous Keap1 protein

To investigate whether HBx promotes the degradation of Keap1 protein, we performed CHX-chase analysis. HepG2 cells were transfected with pEF1A-HBx-Myc-His_6 or the empty plasmid pEF1A-Myc-His_6. The CHX-chase analysis demonstrated no significant difference in the half-life of the endogenous Keapl protein between HBx-Myc-His_6-expressing cells and control cells (Fig. 11A, upper panel, and Fig. 11B). These results suggest that HBx does not affect the half-life of endogenous Keap1 protein.

HBx interacts with Keap1

To determine whether the HBx protein competes with Nrf2 for interaction with Keap1, we performed a coimmunoprecipitation analysis. HepG2 cells were co-transfected with pCAG-FLAG-Keap1 and either pEF1A-HBx-Myc-His_6 or pEF1A-HBc-Myc-His_6. At 48 h after transfection, the cells were harvested, and the cell lysates were immunoprecipitated with anti-Myc beads. Immunoprecipitation analysis revealed that FLAG-Keap1 was coimmunoprecipitated with HBx-Myc-His_6 (Fig. 12A, first panel, lane 5), but not with HBc-Myc-His_6 (Fig. 12A, first panel, lane 6). This result suggests that HBx specifically interacts with Keap1.

To further verify the interaction between HBx and Keap1 in HBV-replicating cells, HepG2 cells were co-transfected with pCAG-FLAG-Keap1 together with either pUC19-HBV-C-AT_JPN or pUC19-HBV-C-AT_JPN(ΔHBx). Immunoprecipitation analysis using anti-FLAG beads showed that HBx (Fig. 12B, first panel, lane 4), but not HBc (Fig. 12B, second panel, lane 4), was coimmunoprecipitated with FLAG-Keap1. No band was detected in HBV-C-AT_JPN(ΔHBx)-replicating cells (Fig. 12B, first panel, lane 5), indicating that the precipitated protein was indeed the HBx protein (Fig. 12B, first panel, lane 4). These results further suggest that HBx specifically interacts with Keap1.

To investigate the interaction between HBx and endogenous Keap1, HepG2 cells were transfected with pEF1A-HBx-Myc-His_6. Consistent with the findings of the above experiments, the immunoprecipitation analysis using anti-Keap1 antibodies showed that HBx-Myc-His_6 was coimmunoprecipitated with endogenous Keap1 (Fig. 12C, first panel, lane 2).

To map the HBx-binding region on Keap1 protein, coimmunoprecipitation analyses were performed using a panel of FLAG-tagged Keap1 deletion mutants (Fig. 12D). The immunoprecipitation analyses revealed that FLAG-Keap1-DGR (double glycine repeat) [amino acid (aa) 315–598], but not FLAG-Keap1-BTB (broad complex, tramtrack, and bric-a-brac) (aa 61–179) or FLAG-Keap1-IVR (intervening region) (aa 180–314), was coimmunoprecipitated with HBx-Myc-His_6 using anti-Myc beads (Fig. 12E, upper right panel, lanes 10–12). These results suggest that the DGR domain of Keap1 is important for HBx binding.

To further investigate whether HBx interferes with the interaction between Nrf2 and Keap1, we performed a proximity ligation assay (PLA) to detect protein-protein interactions as fluorescence signal spots in cells. HepG2 cells were co-transfected with pCAG-FLAG-Nrf2 and pCAG-Keap1, together with either pEGFP-C3 or pEGFP-C3-HBx. The PLA revealed a strong signal in the cytoplasm in the presence of FLAG-Nrf2, Keap1, and EGFP (Fig. 12F, upper panel, Merge). However, expression of EGFP-HBx markedly reduced the PLA signal (Fig. 12F, bottom panel, Merge). These results suggest that HBx interferes with the interaction between Ner2 and Keap1.

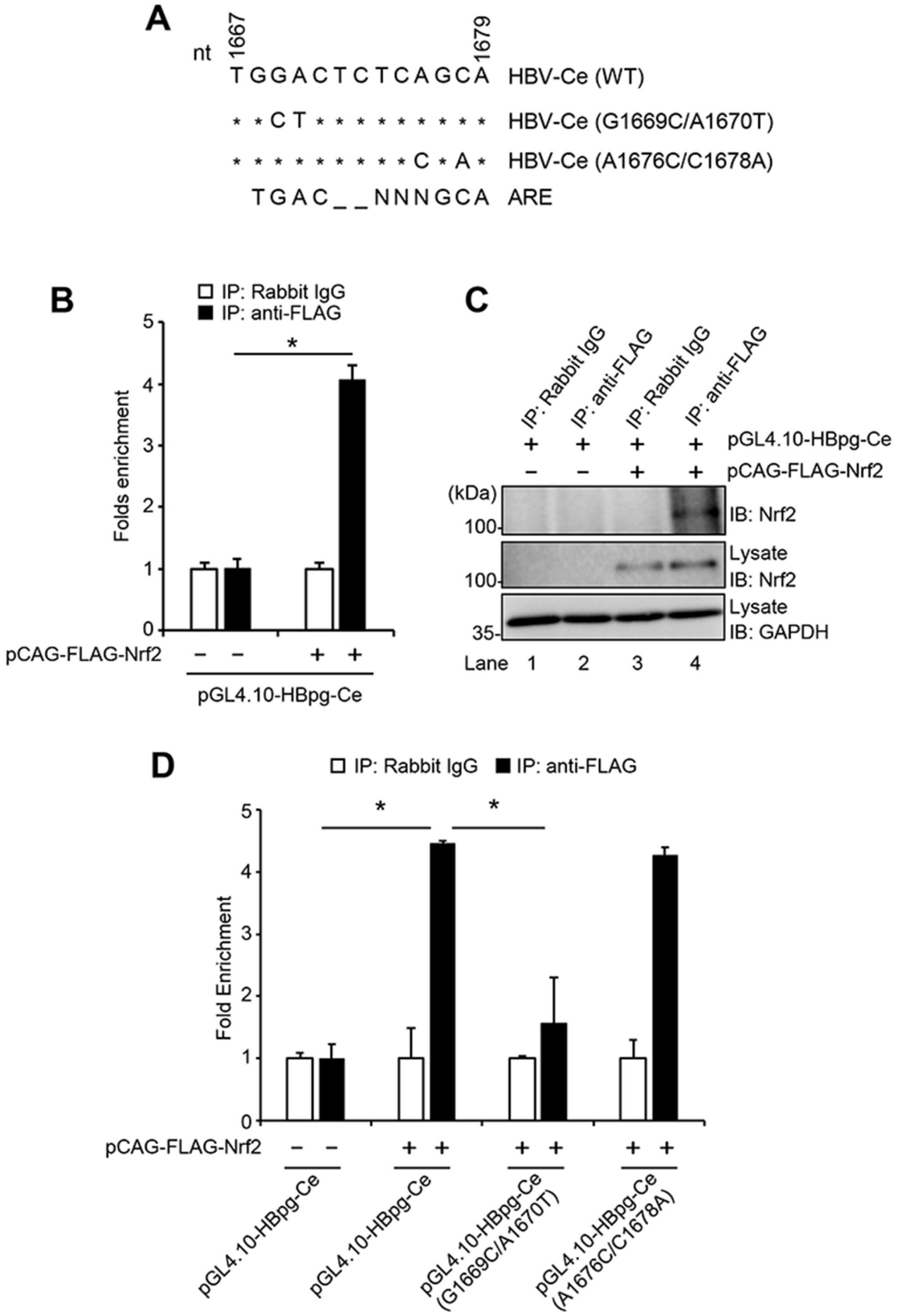

FIG 9 Nrf2 binds to the HBV core promoter. (A) Schematic representation of the putative Nrf2-binding region within the HBV Ce core promoter. Two mutant constructs were prepared by introducing double-point mutations (G1669C/A1670T or A1676C/C1678A) into the ARE sequence in the HBV Ce core promoter. (B) HepG2 cells were transfected with pCAG-FLAG-Nrf2 together with the HBV Ce core promoter reporter plasmid pGL4.10-HBpg-Ce. At 48 h after transfection, the

(Continued on next page)

FIG 9 (Continued)

cells were harvested. Cell lysates were subjected to a ChIP assay using either an isotype control antibody (rabbit IgG) or an anti-FLAG rabbit monoclonal antibody (MAb). Coprecipitated DNA was isolated from the beads, and HBV core promoter DNA was determined by real-time PCR. (C) The amount of immunoprecipitated FLAG-Nrf2 was determined by immunoblotting with anti-Nrf2 MAb (top panel). Input samples were immunoblotted with anti-Nrf2 MAb (middle panel) and anti-glyceraldehyde-3-phosphate dehydrogenase (GAPDH) MAb (bottom panel), respectively. The level of GAPDH served as a loading control. (D) HepG2 cells were transfected with pCAG-FLAG-Nrf2 together with pGL4.10-HBpg-Ce, pGL4.10-HBpg-Ce (G1669C/A1670T), or pGL4.10-HBpg-Ce (A1676C/C1678A). At 48 h after transfection, the cells were harvested. The ChIP assay was performed as described above. The data represent the means ± SEM of data from three independent experiments, and the value for the control cells was arbitrarily expressed as 1.0. *$P < 0.05$.

HBx is colocalized with Keap1 predominantly in the cytoplasm

To examine the subcellular localization of HBx and Keap1, we performed immunofluorescence staining. Huh-7.5 cells were co-transfected with pCAG-FLAG-Keap1 and pEF1A-HBx-Myc-His_6. Immunofluorescence staining revealed that the HBx-Myc-His_6 protein was predominantly colocalized with FLAG-Keap1 in the cytoplasm (Fig. 13A, lower panel, Merge). To further examine whether Keap1 is colocalized with the HBx protein, we performed the PLA. The PLA revealed that a strong signal was observed in the cytoplasm in the presence of both FLAG-Keap1 and HBx-Myc-His_6 (Fig. 13B, bottom panel, Merge). These results suggest that HBx interacts with Keap1 predominantly in the cytoplasm.

Knockdown of Keap1 decreases the levels of intracellular HBV RNA and pgRNA as well as the levels of extracellular HBeAg and HBsAg

To determine the effects of Keap1 on HBV replication, HepG2 cells were transfected with HBV plasmids pUC19-HBV-AeuS, pUC19-HBV-Bj_JPN56, pUC19-HBV-C-AT_JPN, or pUC19-HBV-D-IND60 in the presence or absence of Keap1 siRNA. The intracellular HBV RNA and pgRNA levels were determined by real-time RT-PCR. Knockdown of Keap1 significantly decreased the intracellular HBV RNA and pgRNA levels of HBV-AeuS (Fig. 14A), HBV-Bj_JPN56 (Fig. 14B), HBV-C-AT_JPN (Fig. 14C), and pHBV-D-IND60 (Fig. 14D) compared to the controls. Moreover, an ELISA assay showed that knockdown of Keap1 significantly decreased the amount of extracellular HBeAg (Fig. 14E) and HBsAg (Fig. 14F). These results suggest that Keap1 enhances HBV replication by inhibiting Nrf2 activity.

HBx induces polyubiquitylation of Nrf2 via the K6-linked polyubiquitin chains

To determine the role of HBx in Keap1-mediated Nrf2 polyubiquitylation, we performed a cell-based ubiquitylation assay. HepG2 cells were co-transfected with pEF1A-HBx-Myc-His_6, pCAG-FLAG-Nrf2, pCAG-Keap1, and pRK5-HA-ubiquitin (Ub). At 40 h after transfection, the cells were treated with 25 μM MG132 for 8 h and then harvested. Cell lysates were immunoprecipitated with anti-FLAG beads and immunoblotted with anti-HA polyclonal antibodies to detect ubiquitylated FLAG-Nrf2. The immunoblot revealed that Keap1 enhanced Nrf2-polyubiquitylation (Fig. 15A, first panel, lanes 1 and 2). Moreover, Nrf2-polyubiquitylation was enhanced by HBx in a dose-dependent manner (Fig. 15A, first panel, lanes 3 and 4). This result suggests that HBx plays a role in the enhancement of Nrf2-polyubiquitylation.

To determine the role of HBx in the Nrf2-polyubiquitylation mediated by endogenous Keap1, HepG2 cells were co-transfected with pEF1A-HBx-Myc-His_6, pCAG-FLAG-Nrf2, and pRK5-Ub. Consistent with the findings of the above experiments, the cell-based ubiquitylation assay demonstrated enhanced polyubiquitylation of Nrf2 mediated by endogenous Keap1 in the presence of HBx (Fig. 15B, first panel, lane 2).

To determine the types of polyubiquitin chains on Nrf2, HepG2 cells were co-transfected with pEF1A-HBx-Myc-His_6, pCAG-FLAG-Nrf2, pCAG-Keap1, and a series of ubiquitin K-only constructs. Then, the cell lysates were immunoprecipitated with anti-FLAG beads and immunoblotted with anti-HA polyclonal antibodies to detect ubiquitylated FLAG-Nrf2. Polyubiquitylation of Nrf2 was enhanced by HBx when wild-type (WT)-Ub and K6-Ub were used (Fig. 15C, first panel, lanes 2 and 4). Polyubiquitylation of Nrf2

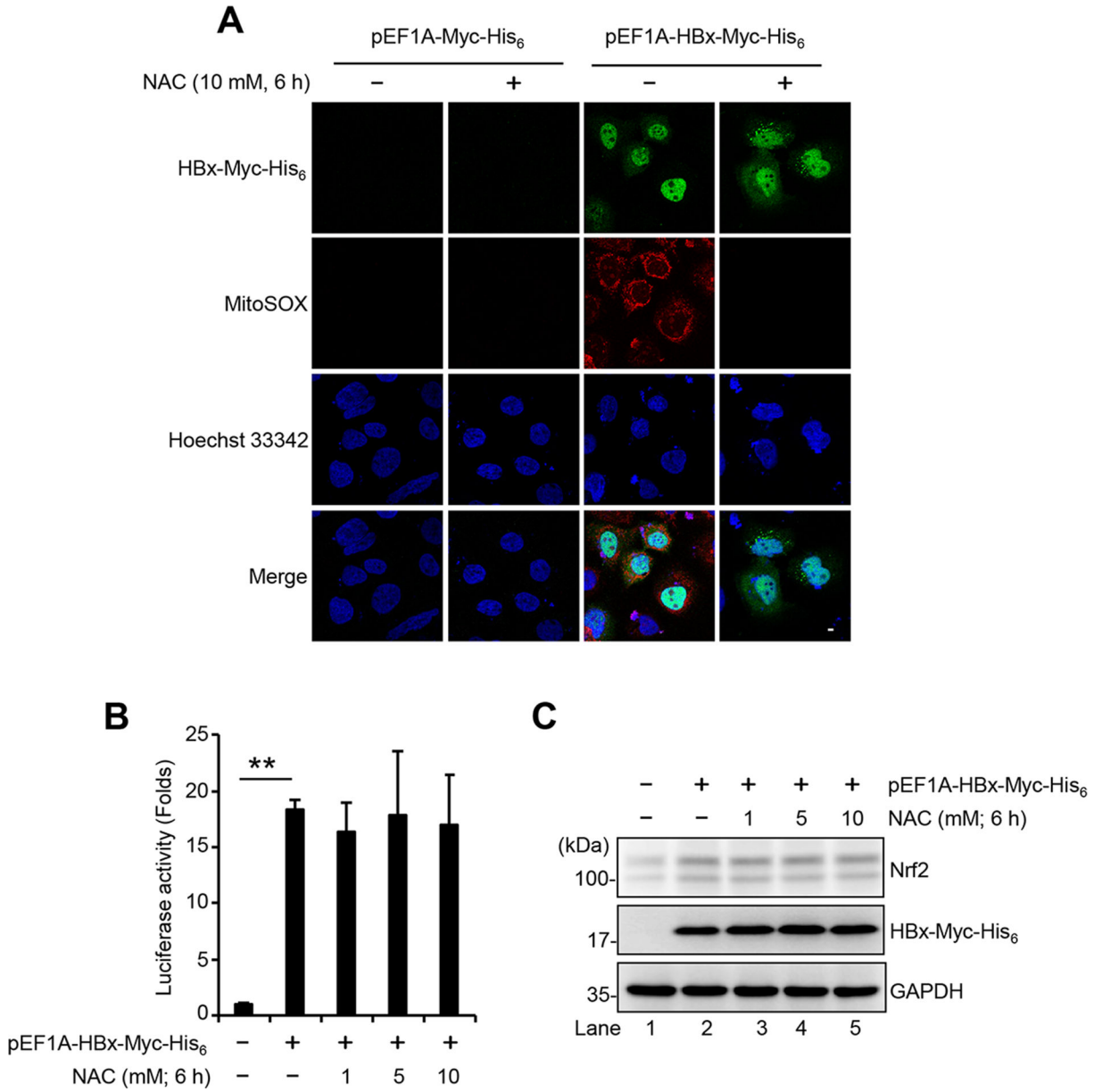

FIG 10 HBx-mediated ROS production is not involved in HBx-induced ARE-luciferase activity. (A) Huh-7.5 cells were transfected with pEF1A-HBx-Myc-His$_6$ or empty plasmid pEF1A-Myc-His$_6$. At 48 h after transfection, the cells were directly incubated with MitoSOX (red, second panel) with or without pretreatment with 10 mM NAC for 6 h and then stained for HBx-Myc-His$_6$ using anti-c-Myc mouse monoclonal antibody (MAb), followed by Alexa Fluor 488-conjugated goat anti-mouse IgG (green, top panel). The cell nuclei were stained with Hoechst 33342 (blue, third panel). Scale bar, 5 µm. (B and C) HepG2 cells were co-transfected with pGL4.37[luc2P/ARE/Hygro] and pEF1A-HBx-Myc-His$_6$. At 48 h after transfection, the cells were harvested with or without pretreatment with 1, 5, or 10 mM antioxidant NAC for 6 h. ARE-luciferase activity was measured and normalized to *Renilla* activity (B). The data represent the means ± SEM of data from three independent experiments, and the value for the control cells was arbitrarily expressed as 1.0. $^{**}P < 0.01$. Cell lysates were analyzed by immunoblotting with anti-Nrf2 MAb (top panel), anti-c-Myc MAb (middle panel), and anti-glyceraldehyde-3-phosphate dehydrogenase (GAPDH) MAb (bottom panel), respectively. The level of GAPDH served as a loading control (C).

was unchanged by co-transfection of the HBx-Myc-His$_6$ plasmid when other ubiquitin plasmids, such as K11-, K27-, K29-, K33-, and K63-Ub, were used (Fig. 15C, lanes 6, 8, 10, 12, 16). Interestingly, polyubiquitylation of Nrf2 by K48-Ub was decreased when the HBx proteins were co-expressed (Fig. 15C, lanes 13 and 14). These results suggest that HBx induces polyubiquitylation of Nrf2 by switching K-48-linked polyubiquitylation to K6-linked polyubiquitylation.

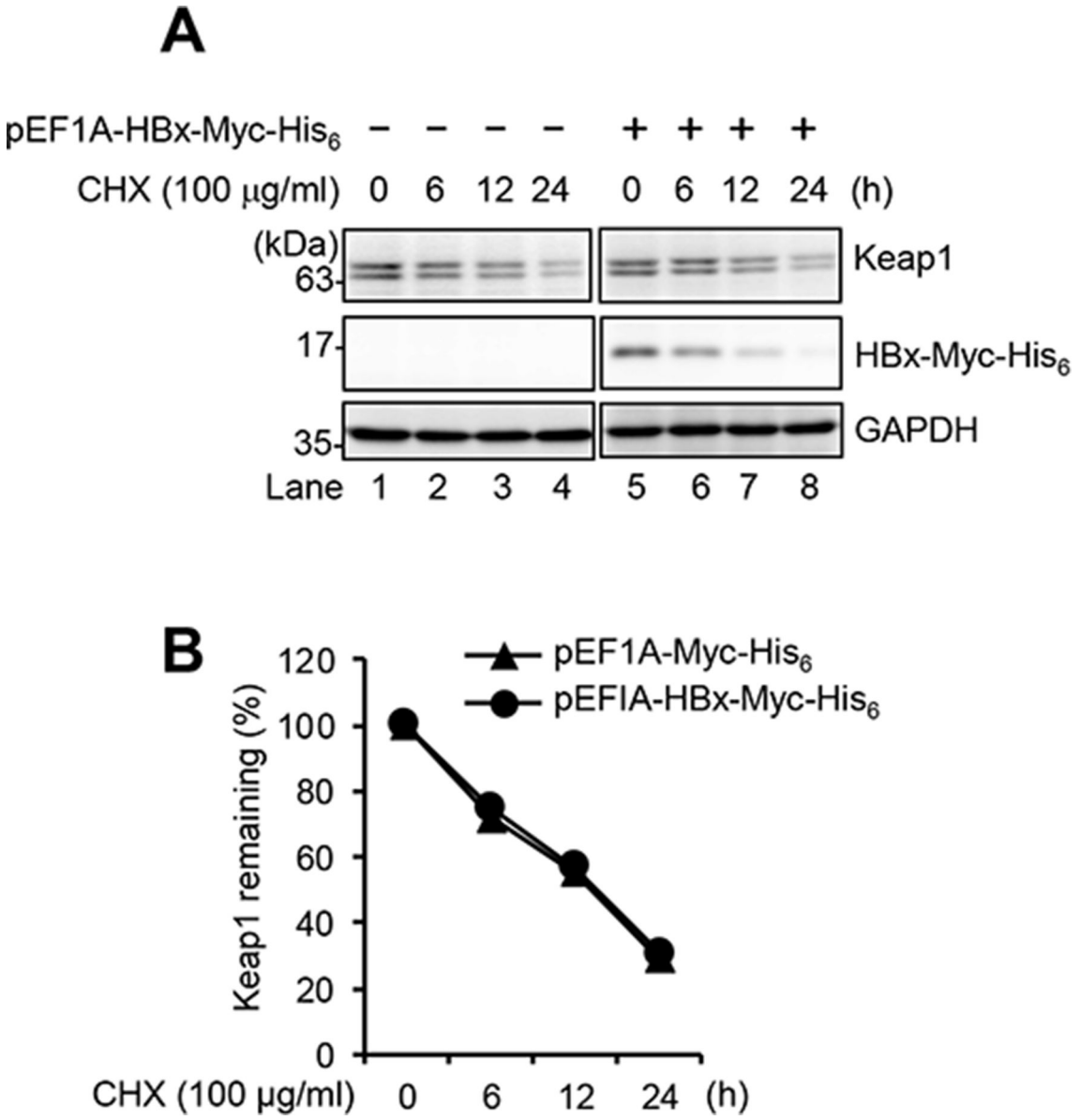

FIG 11 HBx does not affect the half-life of the endogenous Keap1 protein. (A) HepG2 cells were transfected with either pEF1A-HBx-Myc-His$_6$ or the empty plasmid pEF1A-Myc-His$_6$. The cells were treated with 100 μg/mL CHX at 48 h after transfection. The cell lysates were harvested at 0, 6, 12, and 24 h after treatment with CHX. The culture medium was replaced with the medium containing CHX every 6 h, followed by immunoblotting with anti-Keap1 monoclonal antibody (MAb) (first panel), anti-c-Myc MAb (second panel), or anti-glyceraldehyde-3-phosphate dehydrogenase (GAPDH) MAb (third panel). The level of GAPDH served as a loading control. (B) Specific signals were quantitated by densitometry, and the percentage of remaining endogenous Keap1 at each time point was compared with that at the starting point. Closed triangles, pEF1A-Myc-His$_6$; closed circles, pEF1A-HBx-Myc-His$_6$.

The HECT E3 ubiquitin ligase HUWE1 is known to catalyze K6-linked polyubiquitin conjugation. To investigate the effect of HUWE1 on the HBx-induced K6-linked polyubiquitylation of Nrf2, HepG2 cells were co-transfected with pEF1A-HBx-Myc-His$_6$, pCAG-FLAG-Nrf2, and pCAG-Keap1, together with either pRK5-HA-Ub or pRK5-HA-Ub-K6 in the presence or absence of HUWE1 siRNA. Knockdown of HUWE1 decreased HBx-induced enhancement of Nrf2-polyubiquitylation (Fig. 15D, left, first panel, lane 3). Notably, knockdown of HUWE1 resulted in a marked decrease in K6-linked Nrf2-polyubiquitylation (Fig. 15D, right, first panel, lane 6), suggesting that HUWE1 is involved in HBx-induced K6-linked polyubiquitylation of Nrf2.

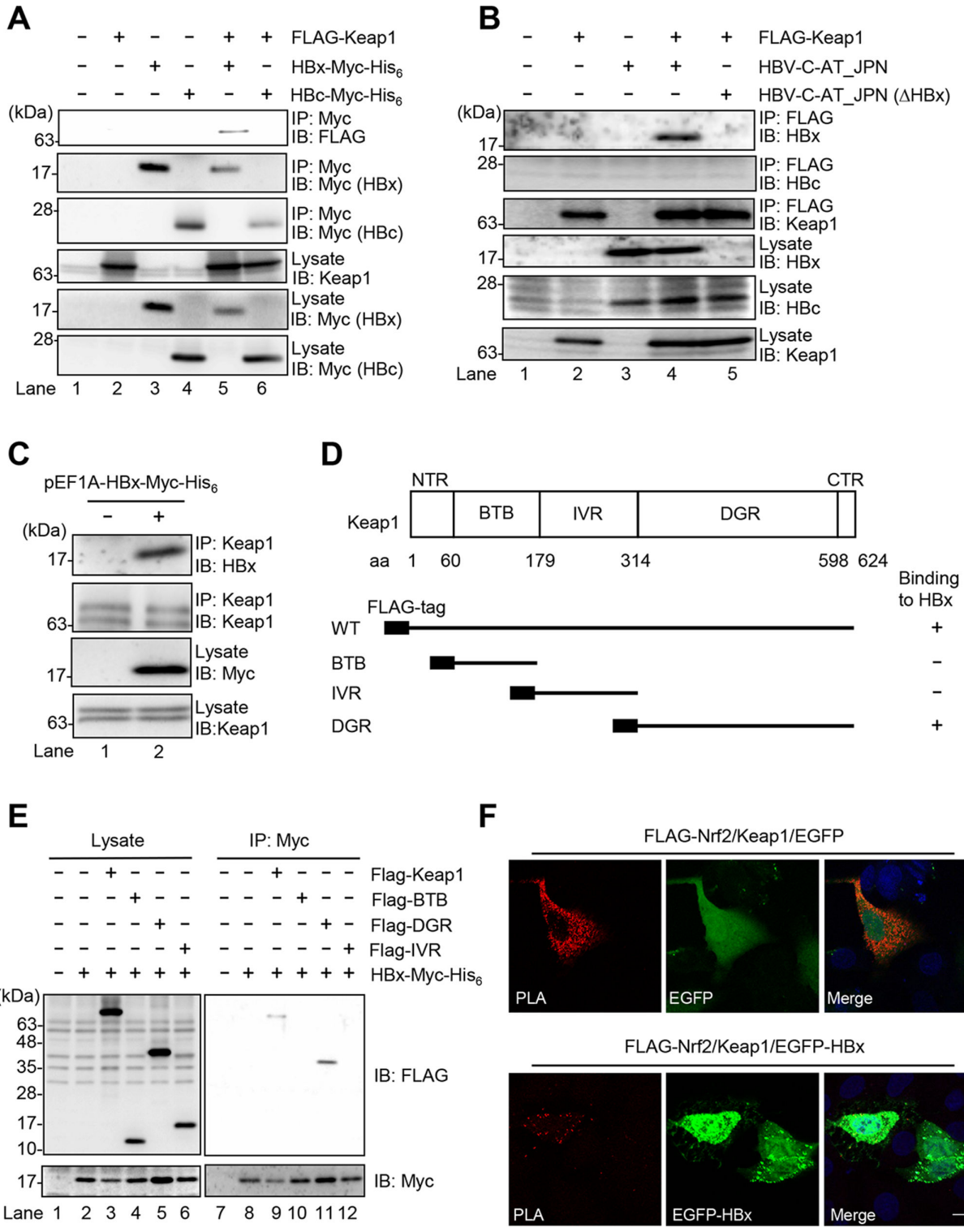

FIG 12 HBx interacts with Keap1. (A) HepG2 cells were transfected with pCAG-FLAG-Keap1 together with either pEF1A-HBx-Myc-His$_6$ or pEF1A-HBc-Myc-His$_6$. At 48 h after transfection, cells were harvested. The cell lysates were immunoprecipitated with anti-Myc beads, followed by immunoblotting with anti-FLAG polyclonal antibody (PAb) (first panel) or anti-c-Myc monoclonal antibody (MAb) (second and third panels). Input samples were immunoblotted with anti-Keap1 MAb (fourth panel) or anti-c-Myc MAb (fifth and sixth panels). (B) HepG2 cells were transfected with pCAG-FLAG-Keap1 together with either pUC19-HBV-C-AT_JPN or pUC19-HBVC-AT_JPN(ΔHBx). At 48 h after transfection, cells were harvested. The cell lysates were immunoprecipitated with anti-FLAG beads, followed by immunoblotting with anti-HBx PAb (first panel), anti-HBc MAb (second panel), or anti-Keap1 MAb (third panel). Input samples were immunoblotted with

(Continued on next page)

FIG 12 (Continued)

anti-HBx PAb (fourth panel), anti-HBc MAb (fifth panel), or anti-Keap1 MAb (sixth panels). (C) HepG2 cells were transfected with pEF1A-HBx-Myc-His_6. At 48 h after transfection, cells were harvested. The cell lysates were immunoprecipitated with an anti-Keap1 mouse MAb antibody, followed by immunoblotting with anti-HBx PAb (first panel) or anti-Keap1 rabbit MAb (second panel). Input samples were immunoblotted with anti-c-Myc MAb (third panel) or anti-Keap1 mouse MAb (fourth panel). (D) Schematic representation of the Keap1 protein. NTR, N-terminal region; BTB, broad complex, tramtrack, and bric-a-brac; IVR, intervening region; DGR, double glycine repeat; CTR, C-terminal region. Each Keap1 deletion mutant contains a FLAG-tag in the N-terminal region. (E) HepG2 cells were transfected with pEF1A-HBx-Myc-His_6 together with each FLAG-Keap1 mutant plasmid as indicated. At 48 h after transfection, cells were harvested. The cell lysates were immunoprecipitated with anti-Myc beads, followed by immunoblotting with anti-FLAG PAb (upper right panel) or anti-c-Myc MAb (lower right panel). Input samples were immunoblotted with anti-FLAG PAb (upper left panel) or anti-c-Myc MAb (lower left panel). (F) HepG2 cells were co-transfected with pCAG-FLAG-Nrf2 and pCAG-Keap1 together with either pEGFP-C3 or pEGFP-C3-HBx. At 48 h after transfection, the cells were fixed, incubated with both anti-Nrf2 rabbit PAb and anti-Keap1 mouse MAb, and subjected to a proximity ligation assay. Scale bar, 10 μm.

Taken together, these results lead us to propose a model in which Keap1 interacts with HBx protein to activate the Nrf2/ARE signaling pathway in HBV-infected cells, in turn leading to an enhanced interaction of Nrf2 with the HBV core promoter and reduced HBV core promoter activity, and finally to the inhibition of hepatitis B virus replication (Fig. 16).

DISCUSSION

In this study, we demonstrated that the Nrf2/ARE signaling pathway was activated by HBV infection (Fig. 1A, B and 3A). HBx played an important role in activation of the Nrf2/ARE signaling pathway (Fig. 1, 3 and 4). Importantly, overexpression of Nrf2 strongly inhibited HBV replication by binding to the HBV core promoter and suppressing its activity (Fig. 5 to 9). To explore the molecular mechanism underlying HBx-mediated Nrf2 activation, we investigated the interaction between HBx and Keap1. An immunoprecipitation assay showed that HBx interacted with Keap1. The DGR domain of Keap1, which mediates interaction with Nrf2 (25), was important for HBx-binding (Fig. 12), suggesting that HBx competes with Nrf2 for interaction with Keap1, promoting nuclear localization and activation of Nrf2. Next, we explored the possible involvement of HBx in Nrf2-polyubiquitylation. Cell-based ubiquitylation assays revealed that HBx promoted polyubiquitylation of Nrf2 by switching from K48-linked polyubiquitylation to K6-linked polyubiquitylation, the latter of which may be associated with Nrf2 stabilization. Collectively, our results suggest that Keap1 recognizes HBx protein to activate the Nrf2/ARE signaling pathway upon HBV infection, leading to an enhanced interaction of Nrf2 with the HBV core promoter and reduced HBV core promoter activity, thereby inhibiting hepatitis B virus replication (Fig. 16). To our knowledge, this is the first study to clarify the role of Nrf2 in the suppression of HBV replication.

It is well known that Nrf2 activation is regulated by both canonical and noncanonical pathways (26). The canonical pathway is activated by the oxidation of cysteine residues in Keap1 in response to oxidative stress or electrophilic chemicals, resulting in Keap1-Cul3 complex inactivation and Nrf2-stabilization (27). Recently, attention has been focused on noncanonical pathway-mediated Nrf2-activation. A set of proteins, such as p62 (28), dipeptidyl peptidase 3 (29), the Wilms tumor gene on the X chromosome (30), PALB2 (31), and BRCA1 (32), interact with Keap1 to disrupt the Keap1-Nrf2 complex, preventing Nrf2 polyubiquitylation and 26S proteasomal degradation, thereby inducing activation of Nrf2. Here, we demonstrated that Keap1 interacted with HBx (Fig. 12). HBx-mediated ROS production is not involved in HBx-induced ARE-luciferase activity (Fig. 10), suggesting that HBx activates Nrf2 via a noncanonical pathway. We propose a model in which the Keap1 dimer forms a complex with HBx, and the HBx in that complex then occupies the Nrf2-binding sites on Keap1, allowing Nrf2 to translocate to the nucleus, leading to Nrf2-activation. We previously reported that Prdx1, a target gene of Nrf2, negatively regulates HBV propagation through the degradation of HBV RNA (33). We therefore propose that Nrf2 inhibits HBV replication via two independent pathways: inhibition of the HBV core promoter activity and enhancement of the level of the antioxidant enzyme Prdx1 to promote degradation of HBV RNA (Fig. 16).

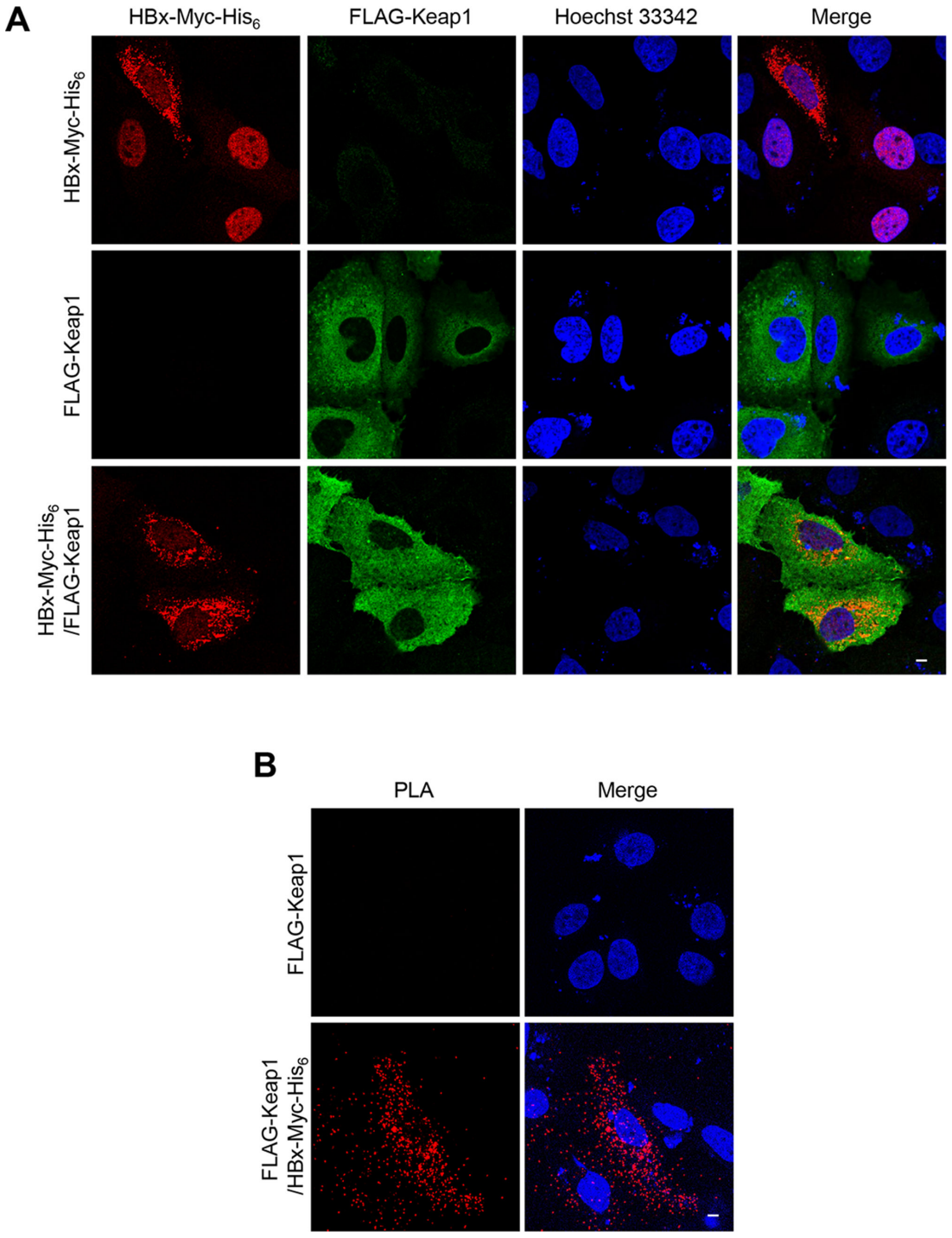

FIG 13 HBx is colocalized with Keap1 predominantly in the cytoplasm. (A) Huh-7.5 cells were transfected with plasmids for HBx-Myc-His_6 (top panel), FLAG-Keap1 (middle panel), or HBx-Myc-His_6 plus FLAG-Keap1 (bottom panel). At 48 h after transfection, the cells were stained with anti-c-Myc mouse monoclonal antibody (MAb), followed by Alexa Fluor 594-conjugated goat anti-mouse IgG (red) and anti-FLAG rabbit polyclonal antibody (PAb), followed by Alexa Fluor 488-conjugated goat anti-rabbit IgG (green). The cell nuclei were stained with Hoechst 33342 (blue). Scale bar, 5 μm. (B) Huh-7.5 cells were transfected with pEF1A-HBx-Myc-His_6 together with pCAG-FLAG-Keap1. At 48 h after transfection, the cells were fixed, incubated with both anti-FLAG rabbit PAb and anti-c-Myc mouse MAb, and subjected to a proximity ligation assay. Scale bar, 5 μm.

Under basal conditions, the Keap1-Cul3 E3 ligase catalyzes Nrf2 via the addition of K48-linked polyubiquitin chains onto Nrf2, thereby targeting it for proteasomal degradation (34). In this study, HBx enhanced the polyubiquitylation of Nrf2 by switching

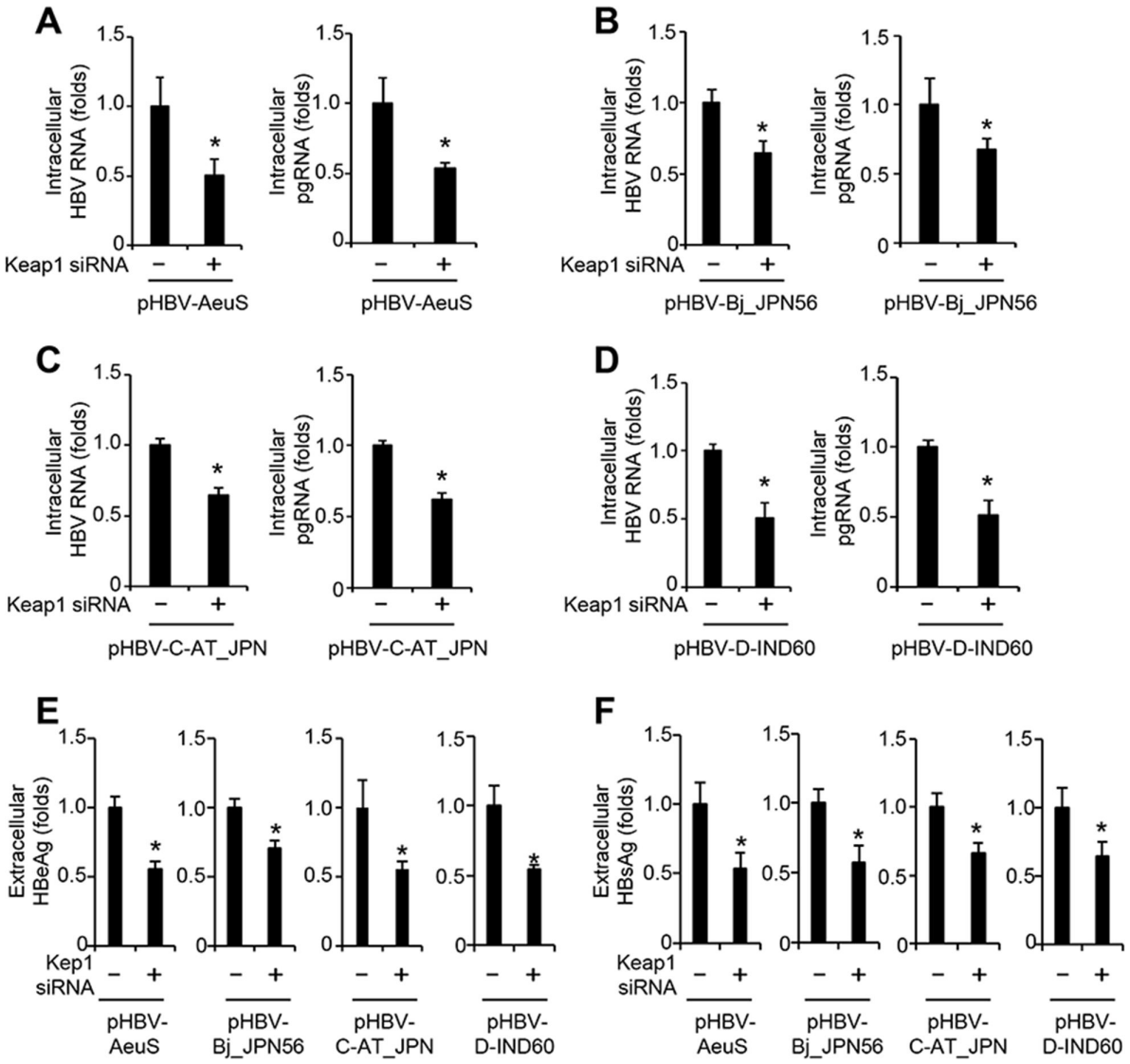

FIG 14 Knockdown of Keap1 decreases the levels of intracellular HBV RNA and pgRNA as well as the levels of extracellular HBeAg and HBsAg. HepG2 cells were transfected with 40 nM Keap1 siRNA. At 24 h after siRNA transfection, the cells were transfected with an HBV expression plasmid that carries the 1.3-mer overlength HBV genome, pUC19-HBV-AeuS (A), pUC19-HBV-Bj_JPN56 (B), pUC19-HBV-C-AT_JPN (C), or pUC19-HBV-D-IND60 (D), followed by incubation for 48 h. Total RNA was extracted 48 h after transfection. The amounts of HBV RNA and pgRNA were quantitated by real-time RT-PCR. The levels of HBeAg (E) and HBsAg (F) in the culture supernatant of HBV-AeuS, HBV-Bj_JPN56, HBV-C-AT_JPN, or HBV-D-IND60-replicating cells were measured by ELISA. The data represent the means ± SEM of data from three independent experiments, and the value for the control cells was arbitrarily expressed as 1.0. *$P < 0.05$, compared with the controls.

K48-linked polyubiquitylation to K6-linked polyubiquitylation (Fig. 15A; Fig. 15C, first panel, lanes 1–4). Although the biological functions of K6-linked polyubiquitin chains have not been clarified, it was reported that the K6-linked polyubiquitin chains of the parkin protein protect it from proteasomal degradation (35). Additionally, we noticed that the Nrf2 protein levels in WT- or K6-Ub-expressing cells were increased in the presence of HBx compared to the controls (Fig. 15C, fourth panel, lanes 1–4). These results suggest that the HBx-induced K6-linked polyubiquitin chains of Nrf2 result in Nrf2 stabilization. Recently, the HECT E3 ubiquitin ligase HUWE1 was reported to catalyze K6-linked polyubiquitin conjugation (36). We demonstrated that knockdown of HUWE1 reduced HBx-induced K6-linked polyubiquitylation of Nrf2 (Fig. 15D, right, first panel, lanes 5 and 6) and HBx-enhanced Nrf2 protein level (Fig. 15D, right, fourth panel, lanes 5

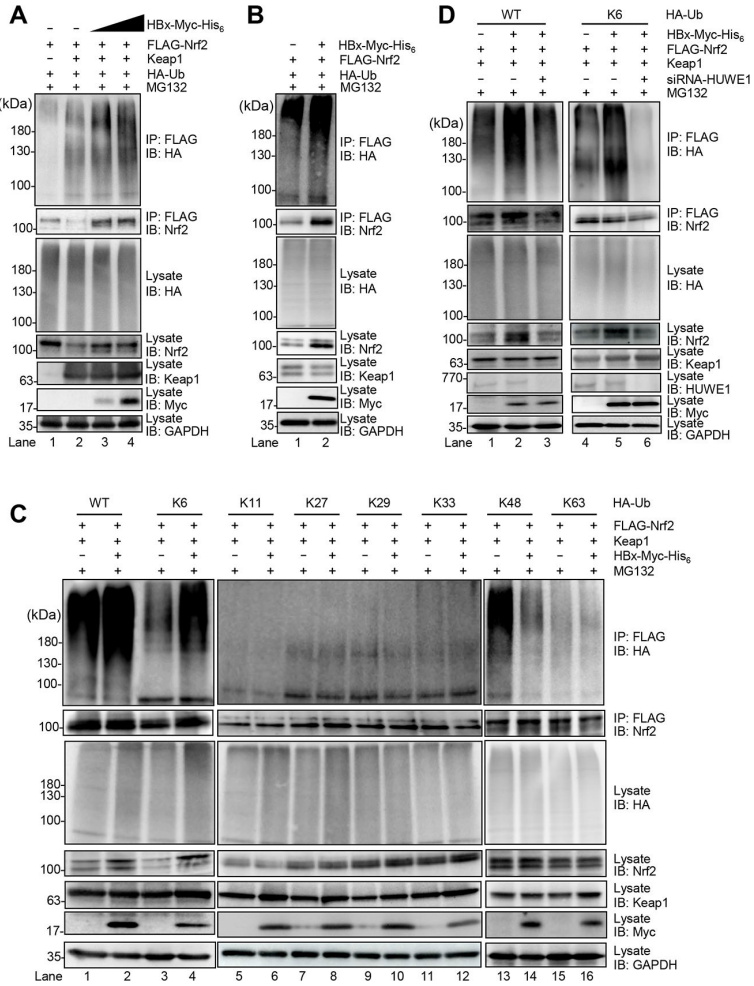

FIG 15 HBx induces polyubiquitylation of Nrf2 via K6-linked polyubiquitin chains. (A) HepG2 cells were co-transfected with pCAG-FLAG-Nrf2, pCAG-Keap1, and pRK5-HA-Ub, together with increasing amounts of pEF1A-HBx-Myc-His_6. At 48 h after transfection, the cells were harvested by treatment with 25 μM MG132 for 8 h. The cell lysates were immunoprecipitated with anti-FLAG beads, followed by immunoblotting with anti-HA polyclonal antibody (PAb) (first panel) or anti-Nrf2 monoclonal antibody (MAb) (second panel). Input samples were immunoblotted with anti-HA PAb (third panel), anti-Nrf2 MAb (fourth panel), anti-Keap1 MAb (fifth panel), anti-c-Myc MAb (sixth panel), or anti-glyceraldehyde-3-phosphate dehydrogenase (GAPDH) MAb (seventh panel). The level of GAPDH served as a loading control. (B) HepG2 cells were co-transfected with pCAG-FLAG-Nrf2, pEF1A-HBx-Myc-His_6, and pRK5-HA-Ub. At 48 h after transfection, the cells were harvested by treatment with 25 μM MG132 for 8 h. The cell lysates were immunoprecipitated with anti-FLAG beads, followed by immunoblotting with anti-HA PAb (first panel) or anti-Nrf2 MAb (second panel). Input samples were immunoblotted with anti-HA PAb (third panel), anti-Nrf2 MAb (fourth panel), anti-Keap1 MAb (fifth panel), anti-c-Myc MAb (sixth panel), or anti-GAPDH MAb (seventh panel). The level of GAPDH served as a loading control. (C) HepG2 cells were co-transfected with pCAG-FLAG-Nrf2, pCAG-Keap1, pEF1A-HBx-Myc-His_6, and the indicated HA-tagged Ub plasmids. At 48 h after transfection, the cells were harvested by treatment with 25 μM MG132 for 8 h. The cell lysates were immunoprecipitated with anti-FLAG beads, followed by immunoblotting with anti-HA PAb (first panel) or anti-Nrf2 MAb (second panel). Input samples were immunoblotted with anti-HA PAb (third panel), anti-Nrf2 MAb (fourth panel), anti-Keap1 MAb (fifth panel), anti-c-Myc MAb (sixth panel), or anti-GAPDH MAb (seventh panel). The level of GAPDH served as a loading control. (D) HepG2 cells were transfected with 40 nM HUWE1 siRNA or control siRNA. At 24 h after siRNA-transfection, cells were co-transfected with pCAG-FLAG-Nrf2, pCAG-Keap1, and pEF1A-HBx-Myc-His_6 together with pRK5-HA-Ub or pRK5-HA-Ub-K6. At 48 h after transfection, the cells were harvested by treatment with 25 μM MG132

(Continued on next page)

FIG 15 (Continued)

for 8 h. The cell lysates were immunoprecipitated with anti-FLAG beads, followed by immunoblotting with anti-HA PAb (first panel) or anti-Nrf2 MAb (second panel). Input samples were immunoblotted with anti-HA PAb (third panel), anti-Nrf2 MAb (fourth panel), anti-Keap1 MAb (fifth panel), anti-HUWE1 PAb (sixth panel), anti-c-Myc MAb (seventh panel), or anti-GAPDH MAb (eighth panel). The level of GAPDH served as a loading control.

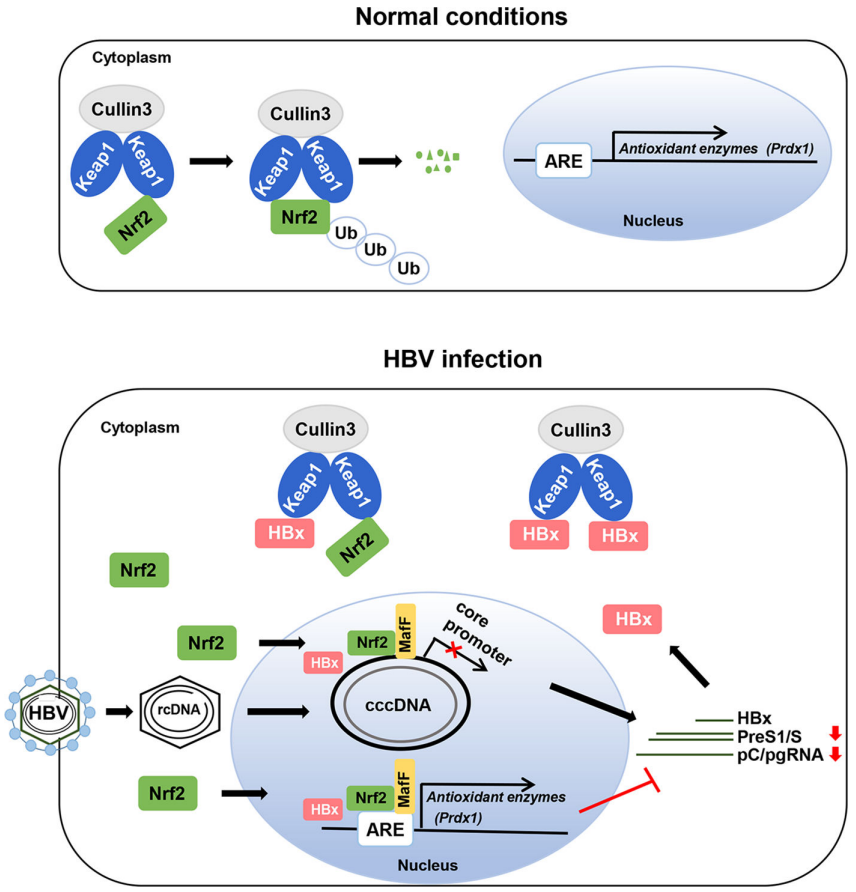

FIG 16 A proposed mechanism of the Keap1/Nrf2/ARE signaling pathway-mediated inhibition of HBV replication. Under normal conditions, Keap1 interacts with Nrf2 in the cytoplasm, leading to ubiquitin-dependent proteasomal degradation of Nrf2. Upon HBV infection, Keap1 interacts with HBx to form an HBx–Keap1 complex and allows Nrf2 to translocate to the nucleus. The activation of Nrf2 inhibits HBV replication by inhibiting HBV core promoter activity and increasing the transcription of the antioxidant enzyme Prdx1 to promote degradation of HBV RNA.

and 6), suggesting that HUWE1 participates in Nrf2-stabilization via K6-linked polyubiquitylation of Nrf2. We are currently investigating whether the Keap1–HBx interaction recruits HUWE1 to catalyze K6-linked polyubiquitylation of Nrf2.

Several studies have demonstrated possible links between Nrf2 and antiviral responses during viral infections. For example, Keap1 interacts with the early accessory protein Rev of the equine infectious anemia virus to activate Nrf2, leading to the enhancement of antiviral defense (37). Keap1 also interacts with the VP24 protein of Marburg virus to activate the cytoprotective antioxidant response pathway via the activation of Nrf2 (38). In addition, herpes simplex virus-1 (HSV-1) activates Nrf2, resulting in restriction of HSV-1 viral infection (39). Although it was previously reported that HBV induces activation of Nrf2 (24, 40), the role of Nrf2 activation in HBV replication was unclear. In this study, we demonstrated that Nrf2 suppressed HBV replication by

binding to the HBV core promoter (Fig. 9) and thereby inhibiting the HBV core promoter activities of HBV genotypes A, B, C, and D (Fig. 8). Our results are consistent with the recent study indicating that MafF, a member of the sMaf protein family, binds to the HBV core promoter and inhibits its transcription (41).

The Nrf2 agonists or activators have been widely used to investigate the antiviral activity of Nrf2. For example, Nrf2 agonists 4-octyl-itaconate and the clinically approved dimethyl fumarate potently inhibit the replication of severe acute respiratory syndrome coronavirus 2 (42). RA-839, a selective agonist of Nrf2, exerts potent anti-rotaviral efficacy (43). The Nrf2 activator hemin, which is a heme oxygenase-1 inducer, efficiently suppresses viral replication of the Ebola virus (44) and Zika virus (45). In addition, the Nrf2 activator bardoxolone methyl reduces the level of intracellular HBV pgRNA (46).

Based on our findings, we propose a model in which Keap1 interacts with HBx protein to activate the Nrf2/ARE signaling pathway upon HBV infection, leading to enhanced interaction of Nrf2 with the HBV core promoter and reduced HBV core promoter activity, thereby inhibiting HBV replication. Our results may lead to a better understanding of the mechanistic details of Nrf2/ARE signaling pathway activation as a host defense mechanism in HBV infection. Nrf2 activation could be a potential target for developing strategies for fighting HBV.

MATERIALS AND METHODS

Cell culture

Human hepatoblastoma HepG2 cells and human hepatoma Huh-7.5 cells (47) (kindly provided by Dr. C. M. Rice, The Rockefeller University, NY, USA) were cultured in Eagle's minimum essential medium with L-glutamine (FUJIFILM Wako Pure Chemical Industries, Osaka, Japan) and Dulbecco's modified Eagle's medium (DMEM) (high glucose) with L-glutamine (FUJIFILM Wako Pure Chemical Industries), respectively, and supplemented with 10% heat-inactivated fetal bovine serum (FBS) (Biowest, Nuaillé, France), 100 units/mL penicillin, 100 µg/mL streptomycin (Gibco, Grand Island, NY, USA), and 0.1 mM nonessential amino acids (Gibco). HepG2-hNTPC-C4 cells (48) were cultured in DMEM/F-12 (Gibco) supplemented with 10% FBS (Biowest), 10 mM HEPES (Gibco), 100 units/mL penicillin, 100 µg/mL streptomycin (Gibco), 5 µg/mL insulin (Sigma, St. Louis, MO, USA), and 400 µg/mL G418 (Nacalai Tesque, Kyoto, Japan). Cells were transfected with plasmid DNA using FuGene 6 transfection reagents (Promega, Madison, WI, USA).

HBV preparation and infection

HBV infection was performed as described previously (49). Briefly, HBV (genotype D) was prepared from the culture supernatant of Hep38.7-Tet cells (50) and concentrated with PEG8000 precipitation. HBV was inoculated into HepG2-hNTCP-C4 cells at 40,000 genome equivalents (GEq)/cell in the presence of 4% PEG8000 at 37°C. Twenty-four hours postinfection, the infected cells were washed with phosphate buffered saline (PBS), followed by the addition of fresh medium.

Expression plasmids

A full-length Nrf2 cDNA was amplified by RT-PCR using the mRNAs of HepG2 cells as a template. The primer sequences were as follows: sense primer, 5′-TCGAGCTCAGCGGCCATGATGGACTTGGAGCTGC-3′ and antisense primer, 5′-AGTGAATTCGCGGCCCTAGTTTTTCTTAACATCTGG-3′. The amplified PCR product was purified and inserted into the NotI site of pCAG-FLAG using an In-Fusion HD cloning kit (Clontech, Mountain View, CA, USA). To generate two sets of Nrf2 siRNA-resistant expression plasmids, pCAG-FLAG-Nrf2-R #7 and pCAG-FLAG-Nrf2-R #10, two silent mutations were introduced in the Nrf2 siRNA target sequence. Nucleotide substitutions were introduced to the wild-type FLAG-Nrf2 expression plasmid by using a QuikChange site-directed mutagenesis kit (Agilent Technologies, Santa Clara, CA, USA).

The primer sequences were as follows: sense primer (FLAG-Nrf2-R #7), 5′-CTAAATGGGCCCATTGATGTATCGGATCTATCACTTTGC-3′; antisense primer (FLAG-Nrf2-R #7), 5′-GCAAAGTGATAGATCCGATACATCAATGGGCCCATTTAG-3′; sense primer (FLAG-Nrf2-R #10), 5′-CAGCAACAGCATGCCCTCACCAGCAACTTTAAGCCATTCAC-3′; and antisense primer (FLAG-Nrf2-R #10), 5′-GTGAATGGCTTAAAGTTGCTGGTGAGGGCATGCTGTTGCTG-3′.

To express FLAG- and HA-tagged or untagged Keap1 proteins, the full-length Keap1 cDNA was amplified by RT-PCR. The primer sequences were as follows: sense primer (FLAG- or HA-tag), 5′-TCGAGCTCAGCGGCCATGCAGCCAGATCCCAGG-3′; antisense primer (FLAG- or HA-tag), 5′-AGTGAATTCGCGGCCTCAACAGGTACAGTTCTGC-3′; sense primer (no tag), 5′-TCGAGCTCAGCGGCCATGCAGCCAGATCCCAGG-3′; and antisense primer (no tag), 5′-AGTGAATTCGCGGCCTCAACAGGTACAGTTCTGCT-3′. The amplified PCR products were inserted into the NotI site of pCAG-FLAG, pCAG-HA, or pCAG using an In-Fusion HD cloning kit.

To express the Keap1 deletion mutants Keap1-BTB (aa 61–179), Keap1-IVR (aa 180–314), and Keap1-DGR (aa 315–598), each fragment was amplified by PCR using pCAG-FLAG-Keap1 as a template and cloned into the NotI site of pCAG-FLAG. The specific primers used for the PCR were as follows: sense primer (Keap1-BTB), 5′-TCGAGCTCAGCGGCCAAGCAGGCCTTTGGCATC-3′; antisense primer (Keap1-BTB), 5′-AGTGAATTCGCGGCCTCACAGCTGCTGCACCAG-3′; sense primer (Keap1-IVR), 5′-TCGAGCTCAGCGGCCGACCCCAGCAATGCCATCG-3′; antisense primer (Keap1-IVR), 5′-AGTGAATTCGCGGCCTCACGTGGGCTTGTGCAG-3′, sense primer (Keap1-DGR), 5′-TCGAGCTCAGCGGCCCAGGTGATGCCCTGCCGG-3′; and antisense primer (Keap1-DGR), 5′-AGTGAATTCGCGGCCTCATGTCATTCGGGTCACC-3′.

The double-point mutant HBV Ce core promoter G1669C/A1670T was constructed by overlap extension PCR using pGL4.10-HBpg-Ce (33) as a template. The specific primers used for PCR were as follows: sense primer, 5′-CTTACATAAGAGGACTCTTGCTCTCTCAGC-AATGTCAACG-3′ and antisense primer, 5′-CGTTGACATTGCTGAGAGAGCAAGAGTCCTCTT-ATGTAAG-3′.

To express the EGFP-tagged HBx protein, the cDNA fragment of HBx was amplified by PCR using pEF1A-HBx-Myc-His_6 as a template and cloned into the XhoI and HindIII sites of pEGFP-C3 (Clontech) using the In-Fusion HD cloning kit, and the resultant plasmid was designated pEGFP-C3-HBx. The specific primers used for the PCR were as follows: sense primer, 5′-TACAAGTACTCAGATCTCGAGATGGCTGCTAGGGTGTGCTGCCAA-3′ and antisense primer, 5′- CTGCAGAATTCGAAGCTTTTAGGCAGAGGTGAAAAAGTTGCATGG-3′.

The HBV expression plasmids pUC19-HBV-AeuS, pUC19-HBV-Bj_JPN56, pUC19-HBV-C-AT_JPN, and pUC19-D-IND60 each carry a 1.3-mer overlength HBV genome (51). The expression plasmids pEF1A-HBx-Myc-His_6, pEF1A-HBc-Myc-His_6, pEF1A-LHBs-Myc-His_6, and pEF1A-HBV Pol-Myc-His_6 (33) and Myc-His_6-tagged HBx expression plasmids from HBV genotypes A, B, C, and D (52) were used. The N-terminal HA-tagged Ub expression plasmids pRK5-HA-Ub-WT, pRK5-HA-Ub-K6, pRK5-HAUb-K11, pRK5-HA-Ub-K27, pRK5-HA-Ub-K29, pRK5-HA-Ub-K33, pRK5-HA-Ub-K48, and pRK5-HA-Ub-K63 (all from Addgene, Watertown, MA, USA) and the plasmids pGL4.10-HBpg-Ce (A1676C/C1678A) (41) and pUC19-HBV-C-AT_JPN(ΔHBx) (53) were also used.

Antibodies

The mouse monoclonal antibodies (MAbs) used in this study were anti-Nrf2 MAb (A-10; sc-365949; Santa Cruz Biotechnology, Santa Cruz, CA, USA), anti-Keap1 MAb (G-2; sc-365626; Santa Cruz Biotechnology), anti-c-Myc MAb (9E10; sc-40; Santa Cruz Biotechnology), anti-HBc MAb (clone 7B2, culture supernatant of the hybridoma) (54, 55), and anti-glyceraldehyde-3-phosphate dehydrogenase (GAPDH) MAb (014-25524; FUJIFILM Wako Pure Chemical Industries). The rabbit MAbs used in this study were anti-Keap1 MAb (D6B12; 8047; Cell Signaling Technology, Beverly, MA, USA), anti-Nrf2 MAb (D1Z9C; 12721S; Cell Signaling Technology), and anti-FLAG MAb (D6W5B; 14793; Cell Signaling Technology). The rabbit polyclonal antibodies (PAbs) used in this study were anti-HA PAb (H-6908; Sigma), anti-FLAG PAb (2368; Cell Signaling Technology),

anti-HBx PAb (ab39716; Abcam, Cambridge, UK), and anti-HUWE1 PAb (ab70161; Abcam). The horse PAb used in this study was anti-HBs (ab9193; Abcam). Horseradish peroxidase (HRP)-conjugated anti-mouse IgG (7076; Cell Signaling Technology), HRP-conjugated anti-rabbit IgG (7074; Cell Signaling Technology), and HRP-conjugated anti-horse IgG (ab6921; Abcam) were used as secondary antibodies.

RNA-Seq analysis

HepG2-hNTCP-C4 cells were infected with HBV at 40,000 GEq/cells. At 12 dpi, total RNA was isolated from HBV-infected cells and mock-infected control cells using the RNeasy Mini Kit (Qiagen, Valencia, CA, USA). Total RNA sequencing was performed by Rhelixa Inc. (Tokyo, Japan). In brief, mRNA was extracted using the NEBNext Poly(A) mRNA Magnetic Isolation Module (E7490; New England Biolabs, Ipswich, MA, USA), followed by cDNA library construction using the NEBNext UltraTMII Directional RNA Library Prep Kit (E7760; New England Biolabs). Subsequently, the libraries underwent sequencing using an Illumina NovaSeq 6,000 sequencer (Illumina, San Diego, CA, USA).

The quality of the raw sequencing data was evaluated using FastQC (version 0.11.7), and adapter sequences were trimmed using Trimmomatic (version 0.38). The resulting trimmed reads were aligned to the hg38 reference genome using HISAT2 (version 2.1.0), and a sorted BAM format file was generated using Samtools (version 1.9). Finally, transcripts per million-normalized read count data were obtained using featureCounts (version 1.6.3). Differential expression analysis was carried out using the DESeq2 package (version 1.24.0). Differentially expressed genes were identified based on the criteria of a $|\log_2 FC| > 0.3$ and a P value < 0.05.

The gene sets of NFE2L2.V2 (M2870) and GOMF_ANTIOXIDANT_ACTIVITY were downloaded from the Molecular Signatures Database (https://www.gsea-msigdb.org/gsea/msigdb/cards/NFE2L2.V2 and https://www.gsea-msigdb.org/gsea/msigdb/cards/GOMF_ANTIOXIDANT_ACTIVITY, respectively). The heatmap was generated using the pheatmap package (version 1.0.12).

Immunoprecipitation

Cultured cells were lysed with a buffer containing 150 mM NaCl, 50 mM Tris-HCl (pH 7.5), 1 mM EDTA (pH 8.0), 0.1% sodium dodecyl sulfate (SDS), 1% sodium deoxycholic acid, 1% Triton X-100, and a protease inhibitor cocktail (Roche) for 30 min on ice. The lysates were centrifuged at 20,400 × g for 15 min at 4°C, and the supernatant was immunoprecipitated with anti-Myc beads (MBL, Nagoya, Japan) or anti-FLAG M2 affinity gel (Sigma) at 4°C overnight. After being washed with the lysis buffer five times, the immunoprecipitates were analyzed by immunoblotting.

Immunoblot analysis

Immunoblot analysis was performed as described previously (33, 56). The cell lysates were separated by SDS-polyacrylamide gel electrophoresis and transferred to a polyvinylidene difluoride membrane (Millipore, Billerica, MA, USA). The membranes were incubated with a primary antibody, followed by incubation with an HRP-conjugated secondary antibody. The positive bands were visualized using enhanced chemiluminescence western blotting detection reagents (GE Healthcare, Buckinghamshire, UK). The intensity of bands was quantified using NIH ImageJ software (Java 1.8.0_112).

Cell-based ubiquitylation assay

Cell-based ubiquitylation assays were performed as described previously (57, 58). Cultured cells were lysed with a buffer containing 120 mM NaCl, 50 mM HEPES (pH 7.2), 1 mM EDTA (pH 8.0), 1% NP-40, 0.5% sodium deoxycholic acid, 10 mM *N*-ethylmalemide (Sigma), and a protease inhibitor cocktail (Roche, Mannheim, Germany) for 30 min on ice. The lysates were centrifuged at 20,400 × g for 10 min at 4°C. To dissociate proteins, 1% SDS was added to the lysates, which were then heated at 100°C for 10 min and

diluted 10-fold with the lysis buffer. FLAG-tagged Nrf2 was immunoprecipitated with anti-FLAG M2 affinity gel (Sigma) at 4°C overnight. Immunoprecipitates were analyzed by immunoblotting using anti-HA PAb to detect ubiquitylated FLAG-tagged Nrf2.

siRNA transfection

HepG2 cells were transfected with 40 nM of Nrf2 siRNA #7 (SI03246950; Qiagen), Nrf2 siRNA #10 (SI04320904; Qiagen), Nrf1 siRNA (L-019733-00-0005; Dharmacon, Lafayette, CO, USA), Keap1 siRNA (SI04267886; Qiagen), or HUWE1 siRNA (SI00757862; Qiagen) using Lipofectamine RNAiMAX transfection reagent (Life Technologies, Carlsbad, CA, USA) according to the manufacturer's instructions. Allstars negative control siRNA (Qiagen) was used as a control. All siRNAs were transfected into cells once.

CHX-chase experiment

To examine the half-life of the Nrf2 protein, HepG2 cells were transfected with pCAG-FLAG-Nrf2. At 48 h after transfection, cells were treated with 50 µg/mL CHX (Sigma). The cells at time point zero were harvested immediately after treatment with CHX. Cells from subsequent time points were incubated in a medium containing CHX at 37°C for 0, 5, 15, and 30 min. To examine the half-life of endogenous Nrf2 protein, HepG2 cells were treated with 50 µg/mL CHX and harvested at 0, 0.25, 0.5, 1, and 2 h. To examine the half-life of endogenous Keap1 protein, HepG2 cells were treated with 100 µg/mL CHX. The culture medium was replaced with the fresh medium containing CHX every 6 h. CHX-treated cells were harvested at 0, 6, 12, and 24 h and processed for immunoblot analysis.

RNA extraction and real-time RT-PCR

Total RNA was isolated by using a ReliaPrep RNA cell miniprep system (Promega) according to the manufacturer's instructions, and cDNA was generated by using a GoScript reverse transcription system (Promega). Real-time RT-PCR was performed using TB Green Premix Ex Taq II (TaKaRa Bio, Kyoto, Japan) with SYBR green chemistry on a StepOnePlus real-time PCR system (Applied Biosystems, Foster City, CA, USA). The primer sequences were as follows: HBV (amplify all HBV transcripts except the 0.8 kb transcript encoding HBx) (59), 5′-GCTTTCACTTTCTCGCCAAC-3′ and 5′-GAGTTCCGCAGTATGGATCG-3′; HBV pgRNA (41), 5′-ACTGTTCAAGCCTCCAAGCTGT-3′ and 5′-GAAGGCAAAAACGAGAGTAACTCCAC-3′; Nrf2, 5′-TACTCCCAGGTTGCCCACA-3′ and 5′-CATCTACAAACGGGAATGTCTGC-3′; NQO1, 5′-GGGCAAGTCCATCCCAACTG-3′ and 5′-GCAAGTCAGGGAAGCCTGGA-3′; Prdx1, 5′-CAGCCTGTCTGACTACAAAGGA-3′ and 5′-CCAGTCCTCCTTGTTTCTTAGG-3′; and Nrf1, 5′-GGAGGAGTTCAATGAACTGCTGTC-3′ and 5′-CTCTGGACCTTCTGCTTCATCTGT-3′. As an internal control, human GAPDH gene expression levels were measured using the primers 5′-GCCATCAATGACCCCTTCATT-3′ and 5′- TCTCGCTCCTGGAAGATGG -3′.

ChIP assay

ChIP assays were performed as described previously (41). HepG2 cells were transfected with pCAG-FLAG-Nrf2 together with the HBV Ce core promoter reporter plasmid pGL4.10-HBpg-Ce or either of the mutated HBV Ce core promoter plasmids pGL4.10-HBpg-Ce (G1669C/A1670T) or pGL4.10-HBpg-Ce (A1676C/C1678A). At 48 h after transfection, ChIP was carried out using a SimpleChiP kit (56383; Cell Signaling Technology) according to the manufacturer's instructions. Rabbit anti-FLAG MAb was used for immunoprecipitation. The pelleted beads were subjected to DNA isolation. The resulting output protein and DNA samples were used for immunoblotting and real-time PCR, respectively. The primer sequences for real-time PCR were as follows: HBV core promoter, 5′-TCGCTTCACCTCTGCACGTC-3′ and 5′-GAACATGAGATGATTAGGC-3′.

Luciferase reporter assay

The plasmid pGL4.37[luc2P/ARE/Hygro] (Promega) contains four copies of an ARE that drives transcription of the luciferase reporter gene *luc2P* (*Photinus pyralis*). The firefly luciferase reporter plasmids carrying the entire HBV Ce core promoter [nt 900 to 1,851; a nonsense mutation (ATG to TAG at nt 1,374 to 1,376) was introduced at the start codon of the HBx gene], Enh1/X promoter (nt 950 to 1,373), preS1 promoter (nt 2,707 to 2,847), or preS2/S promoter (nt 2,937 to 3,204) were used (33). The entire HBV core promoter from genotypes A, B, and D reporter luciferase plasmids pGL4.10-HBpg-Aa, pGL4.10-HBpg-Bj, and pGL4.10-HBpg-D were constructed as reported previously (33). The plasmid pRL-CMV-Renilla (Promega), which expresses *Renilla* luciferase, was used as an internal control. HepG2 cells cultured in a 24-well plate were transiently transfected with the reporter constructs described above. At 48 h after transfection, the cells were harvested, and a luciferase assay was performed using a dual-luciferase reporter assay system (Promega). Firefly and *Renilla* luciferase activities were measured with a GloMax 96 microplate luminometer (Promega). Firefly luciferase activity was normalized to *Renilla* luciferase activity for each sample.

Detection of mitochondrial superoxide

Cells seeded on glass coverslips in a 24-well plate were incubated with 5 μM MitoSOX Red (Molecular Probes, Eugene, OR, USA) at 37°C for 10 min. After being washed with warm Hanks' balanced salt solution with calcium and magnesium (Invitrogen, Carlsbad, CA, USA), the cells were fixed with 4% paraformaldehyde and subjected to indirect immunofluorescence as described below. The stained cells were observed under a confocal laser scanning microscope (LSM700; Carl Zeiss, Oberkochen, Germany).

Indirect immunofluorescence staining

Indirect immunofluorescence staining was performed as described previously (56). Briefly, Huh-7.5 or HepG2 cells seeded on glass coverslips in a 24-well plate were fixed with 4% paraformaldehyde for 15 min at room temperature and permeabilized in 0.1% Triton X-100 in PBS for 15 min at room temperature. After being washed with PBS twice, cells were stained with primary and secondary antibodies. The primary antibodies used were anti-c-Myc mouse MAb and anti-FLAG rabbit PAb. The secondary antibodies used were Alexa Fluor 594-conjugated goat anti-mouse IgG (A11005; Molecular Probes) and Alexa Fluor 488-conjugated goat anti-rabbit IgG (A11008; Molecular Probes). The stained cells were observed under a confocal laser scanning microscope (LSM700; Carl Zeiss).

Proximity ligation assay

In situ PLA was performed using a Duolink In Situ PLA Kit (Sigma) as described previously (60). Briefly, Huh-7.5 cells seeded on glass coverslips were transfected with the plasmid pEF1A-HBx-Myc-His_6 together with pCAG-FLAG-Keap1. At 48 h after transfection, the cells were fixed with 4% paraformaldehyde for 15 min and permeabilized with PBS containing 0.1% Triton X-100 for 15 min at room temperature. The coverslips were incubated with anti-c-Myc mouse MAb and anti-FLAG rabbit PAb. The samples were washed three times with the wash buffer from the kit. The PLA probes, i.e., anti-mouse MINUS and anti-rabbit PLUS, were diluted in the antibody diluent provided with the kit. The samples were incubated for 1 h at 37°C in a humidity chamber. To assess the interaction between Keap1 and Nrf2, HepG2 cells seeded on glass coverslips were co-transfected with pCAG-Keap1 and pCAG-FLAG-Nrf2, together with either pEGFP-C3 or pEGFP-C3-HBx. At 48 h after transfection, the cells were fixed and permeabilized as described above. The coverslips were incubated with anti-Keap1 mouse MAb and anti-Nrf2 rabbit MAb. The PLA probes, anti-mouse MINUS and anti-rabbit PLUS, were used for a 1-h incubation at 37°C. The samples were washed and processed according to the manufacturer's instructions for probe ligation, signal amplification, and mounting. The samples were examined with a confocal microscope (LSM 700; Carl Zeiss).

Detection of HBsAg and HBeAg

The levels of HBsAg and HBeAg in the culture medium were measured by ELISA kits according to the manufacturer's instructions (HBsAg: DIA source, Rue du Bosquet, Belgium; HBeAg: LifeSpan Bio Sciences, Seattle, WA, USA).

Statistical analysis

Results were expressed as means ± standard errors of the means. Statistical significance was evaluated by analysis of variance and was defined as a P value of < 0.05.

ACKNOWLEDGMENTS

We thank Y. Kozaki for the secretarial work. We also thank S.A. Setiawan and C.-T. Yeh from Taipei Medical University, Taipei, Taiwan, for their technical assistance.

This work was supported by the Program for Basic and Clinical Research on Hepatitis from the Japan Agency for Medical Research and Development (AMED) under grant no. 23fk0310507h0002 and by a grant from the KAKENHI under grant number 21K07040. A.A. is supported by the Program for Nurture of Next Generation Leaders Guiding Medical Innovation in Asia of the Ministry of Education, Culture, Sports, Science, and Technology (MEXT) of Japan.

A.A., L.D., and I.S. conceived and designed the experiments. A.A. and L.D. carried out most of the experiments. T.A. and C.M. assisted with the construction and the data analysis. M.I., A.R., H.A., K.W., T.S., M.M., and Y.M. contributed to the materials. A.A., L.D., and I.S. wrote the manuscript.

AUTHOR AFFILIATIONS

[1]Division of Infectious Disease Control, Center for Infectious Diseases, Kobe University Graduate School of Medicine, Kobe, Japan
[2]Faculty of Medicine, Public Health and Nursing, Universitas Gadjah Mada, Yogyakarta, Indonesia
[3]Department of Virology and Parasitology, Hamamatsu University School of Medicine, Hamamatsu, Japan
[4]Department of Virology III, National Institute of Infectious Diseases, Tokyo, Japan
[5]Department of Virology II, National Institute of Infectious Diseases, Tokyo, Japan
[6]Research Center for Drug and Vaccine Development, National Institute of Infectious Diseases, Tokyo, Japan
[7]Research Center for Hepatitis and Immunology, National Center for Global Health and Medicine, Ichikawa, Japan
[8]Center for Infectious Disease Education and Research (CiDER), Osaka University, Osaka, Japan
[9]Laboratory of Virus Control, Research Institute for Microbial Diseases (RIMD), Osaka University, Osaka, Japan

AUTHOR ORCIDs

Ikuo Shoji http://orcid.org/0000-0002-0730-4379

FUNDING

Funder	Grant(s)	Author(s)
Japan Agency for Medical Research and Development (AMED)	23fk0310507h0002	Ikuo Shoji
MEXT | Japan Society for the Promotion of Science (JSPS)	21K07040	Lin Deng

AUTHOR CONTRIBUTIONS

Adi Ariffianto, Conceptualization, Investigation, Writing – original draft | Lin Deng, Conceptualization, Investigation, Validation, Writing – original draft | Takayuki Abe, Investigation, Validation | Chieko Matsui, Investigation, Validation | Masahiko Ito, Resources | Akihide Ryo, Resources | Hussein Hassan Aly, Resources | Koichi Watashi, Resources | Tetsuro Suzuki, Resources | Masashi Mizokami, Resources | Yoshiharu Matsuura, Resources | Ikuo Shoji, Conceptualization, Funding acquisition, Supervision, Writing – original draft, Writing – review and editing

REFERENCES

1. Llovet JM, Zucman-Rossi J, Pikarsky E, Sangro B, Schwartz M, Sherman M, Gores G. 2016. Hepatocellular carcinoma. Nat Rev Dis Primers 2:16018. https://doi.org/10.1038/nrdp.2016.18
2. Organization WH. 2022. Hepatitis B. World Health Organization. Available from: https://www.who.int/news-room/fact-sheets/detail/hepatitis-b
3. Fanning GC, Zoulim F, Hou J, Bertoletti A. 2019. Therapeutic strategies for hepatitis B virus infection: towards a cure. Nat Rev Drug Discov 18:827–844. https://doi.org/10.1038/s41573-019-0037-0
4. Yuen MF, Chen DS, Dusheiko GM, Janssen HLA, Lau DTY, Locarnini SA, Peters MG, Lai CL. 2018. Hepatitis B virus infection. Nat Rev Dis Primers 4:18035. https://doi.org/10.1038/nrdp.2018.35
5. Brownlee M. 2001. Biochemistry and molecular cell biology of diabetic complications. Nature 414:813–820. https://doi.org/10.1038/414813a
6. Gorrini C, Harris IS, Mak TW. 2013. Modulation of oxidative stress as an anticancer strategy. Nat Rev Drug Discov 12:931–947. https://doi.org/10.1038/nrd4002
7. Barnham KJ, Masters CL, Bush AI. 2004. Neurodegenerative diseases and oxidative stress. Nat Rev Drug Discov 3:205–214. https://doi.org/10.1038/nrd1330
8. Sies H, Berndt C, Jones DP. 2017. Oxidative stress. Annu Rev Biochem 86:715–748. https://doi.org/10.1146/annurev-biochem-061516-045037
9. Halliwell B. 1999. Antioxidant defence mechanisms: from the beginning to the end (of the beginning). Free Radic Res 31:261–272. https://doi.org/10.1080/10715769900300841
10. Nguyen T, Nioi P, Pickett CB. 2009. The Nrf2-antioxidant response element signaling pathway and its activation by oxidative stress. J Biol Chem 284:13291–13295. https://doi.org/10.1074/jbc.R900010200
11. Suzuki T, Yamamoto M. 2015. Molecular basis of the Keap1-Nrf2 system. Free Radic Biol Med 88:93–100. https://doi.org/10.1016/j.freeradbiomed.2015.06.006
12. Baird L, Yamamoto M. 2020. The molecular mechanisms regulating the Keap1-Nrf2 pathway. Mol Cell Biol 40:e00099-20. https://doi.org/10.1128/MCB.00099-20
13. Yuan K, Lei Y, Chen HN, Chen Y, Zhang T, Li K, Xie N, Wang K, Feng X, Pu Q, Yang W, Wu M, Xiang R, Nice EC, Wei Y, Huang C. 2016. HBV-induced ROS accumulation promotes hepatocarcinogenesis through snail-mediated epigenetic silencing of SOCS3. Cell Death Differ 23:616–627. https://doi.org/10.1038/cdd.2015.129
14. Tsai SM, Lin SK, Lee KT, Hsiao JK, Huang JC, Wu SH, Ma H, Wu SH, Tsai LY. 2009. Evaluation of redox statuses in patients with hepatitis B virus-associated hepatocellular carcinoma. Ann Clin Biochem 46:394–400. https://doi.org/10.1258/acb.2009.009029
15. Ivanov AV, Valuev-Elliston VT, Tyurina DA, Ivanova ON, Kochetkov SN, Bartosch B, Isaguliants MG. 2017. Oxidative stress, a trigger of hepatitis C and B virus-induced liver carcinogenesis. Oncotarget 8:3895–3932. https://doi.org/10.18632/oncotarget.13904
16. Kitada T, Seki S, Iwai S, Yamada T, Sakaguchi H, Wakasa K. 2001. In situ detection of oxidative DNA damage, 8-hydroxydeoxyguanosine, in chronic human liver disease. J Hepatol 35:613–618. https://doi.org/10.1016/s0168-8278(01)00171-4
17. Higgs MR, Chouteau P, Lerat H. 2014. Liver let die': oxidative DNA damage and hepatotropic viruses. J Gen Virol 95:991–1004. https://doi.org/10.1099/vir.0.059485-0
18. Severi T, Ying C, Vermeesch JR, Cassiman D, Cnops L, Verslype C, Fevery J, Arckens L, Neyts J, van Pelt JF. 2006. Hepatitis B virus replication causes oxidative stress in HepAD38 liver cells. Mol Cell Biochem 290:79–85. https://doi.org/10.1007/s11010-006-9167-x
19. Lee YI, Hwang JM, Im JH, Lee YI, Kim NS, Kim DG, Yu DY, Moon HB, Park SK. 2004. Human hepatitis B virus-X protein alters mitochondrial function and physiology in human liver cells. J Biol Chem 279:15460–15471. https://doi.org/10.1074/jbc.M309280200
20. Waris G, Huh KW, Siddiqui A. 2001. Mitochondrially associated hepatitis B virus X protein constitutively activates transcription factors STAT-3 and NF-kappa B via oxidative stress. Mol Cell Biol 21:7721–7730. https://doi.org/10.1128/MCB.21.22.7721-7730.2001
21. Jung SY, Kim YJ. 2013. C-terminal region of HBx is crucial for mitochondrial DNA damage. Cancer Lett 331:76–83. https://doi.org/10.1016/j.canlet.2012.12.004
22. Lee IK, Lee SA, Kim H, Won YS, Kim BJ. 2015. Induction of endoplasmic reticulum-derived oxidative stress by an occult infection related S surface antigen variant. World J Gastroenterol 21:6872–6883. https://doi.org/10.3748/wjg.v21.i22.6872
23. Lee H, Kim H, Lee SA, Won YS, Kim HI, Inn KS, Kim BJ. 2015. Upregulation of endoplasmic reticulum stress and reactive oxygen species by naturally occurring mutations in hepatitis B virus core antigen. J Gen Virol 96:1850–1854. https://doi.org/10.1099/vir.0.000134
24. Schaedler S, Krause J, Himmelsbach K, Carvajal-Yepes M, Lieder F, Klingel K, Nassal M, Weiss TS, Werner S, Hildt E. 2010. Hepatitis B virus induces expression of antioxidant response element-regulated genes by activation of Nrf2. J Biol Chem 285:41074–41086. https://doi.org/10.1074/jbc.M110.145862
25. Tong KI, Katoh Y, Kusunoki H, Itoh K, Tanaka T, Yamamoto M. 2006. Keap1 recruits Neh2 through binding to ETGE and DLG motifs: characterization of the two-site molecular recognition model. Mol Cell Biol 26:2887–2900. https://doi.org/10.1128/MCB.26.8.2887-2900.2006
26. Silva-Islas CA, Maldonado PD. 2018. Canonical and non-canonical mechanisms of Nrf2 activation. Pharmacol Res 134:92–99. https://doi.org/10.1016/j.phrs.2018.06.013
27. Wakabayashi N, Dinkova-Kostova AT, Holtzclaw WD, Kang MI, Kobayashi A, Yamamoto M, Kensler TW, Talalay P. 2004. Protection against electrophile and oxidant stress by induction of the phase 2 response: fate of cysteines of the Keap1 sensor modified by inducers. Proc Natl Acad Sci U S A 101:2040–2045. https://doi.org/10.1073/pnas.0307301101
28. Komatsu M, Kurokawa H, Waguri S, Taguchi K, Kobayashi A, Ichimura Y, Sou Y-S, Ueno I, Sakamoto A, Tong KI, Kim M, Nishito Y, Iemura S, Natsume T, Ueno T, Kominami E, Motohashi H, Tanaka K, Yamamoto M. 2010. The selective autophagy substrate p62 activates the stress responsive transcription factor Nrf2 through inactivation of Keap1. Nat Cell Biol 12:213–223. https://doi.org/10.1038/ncb2021
29. Hast BE, Goldfarb D, Mulvaney KM, Hast MA, Siesser PF, Yan F, Hayes DN, Major MB. 2013. Proteomic analysis of ubiquitin ligase Keap1 reveals associated proteins that inhibit Nrf2 ubiquitination. Cancer Res 73:2199–2210. https://doi.org/10.1158/0008-5472.CAN-12-4400
30. Camp ND, James RG, Dawson DW, Yan F, Davison JM, Houck SA, Tang X, Zheng N, Major MB, Moon RT. 2012. Wilms tumor gene on X chromosome (WTX) inhibits degradation of Nrf2 protein through competitive binding to KeaP1 protein. J Biol Chem 287:6539–6550. https://doi.org/10.1074/jbc.M111.316471
31. Ma J, Cai H, Wu T, Sobhian B, Huo Y, Alcivar A, Mehta M, Cheung KL, Ganesan S, Kong A-NT, Zhang DD, Xia B. 2012. PALB2 interacts with

Keap1 to promote Nrf2 nuclear accumulation and function. Mol Cell Biol 32:1506–1517. https://doi.org/10.1128/MCB.06271-11
32. Gorrini C, Baniasadi PS, Harris IS, Silvester J, Inoue S, Snow B, Joshi PA, Wakeham A, Molyneux SD, Martin B, Bouwman P, Cescon DW, Elia AJ, Winterton-Perks Z, Cruickshank J, Brenner D, Tseng A, Musgrave M, Berman HK, Khokha R, Jonkers J, Mak TW, Gauthier ML. 2013. BRCA1 interacts with Nrf2 to regulate antioxidant signaling and cell survival. J Exp Med 210:1529–1544. https://doi.org/10.1084/jem.20121337
33. Deng L, Gan X, Ito M, Chen M, Aly HH, Matsui C, Abe T, Watashi K, Wakita T, Suzuki T, Okamoto T, Matsuura Y, Mizokami M, Shoji I, Hotta H. 2019. Peroxiredoxin 1, a novel HBx-interacting protein, interacts with exosome component 5 and negatively regulates hepatitis B virus (HBV) propagation through degradation of HBV RNA. J Virol 93:e02203-18. https://doi.org/10.1128/JVI.02203-18
34. Villeneuve NF, Lau A, Zhang DD. 2010. Regulation of the Nrf2-Keap1 antioxidant response by the ubiquitin proteasome system: an insight into cullin-ring ubiquitin ligases. Antioxid Redox Signal 13:1699–1712. https://doi.org/10.1089/ars.2010.3211
35. Durcan TM, Tang MY, Pérusse JR, Dashti EA, Aguileta MA, McLelland G-L, Gros P, Shaler TA, Faubert D, Coulombe B, Fon EA. 2014. USP8 regulates mitophagy by removing K6-linked ubiquitin conjugates from parkin. EMBO J 33:2473–2491. https://doi.org/10.15252/embj.201489729
36. Michel MA, Swatek KN, Hospenthal MK, Komander D. 2017. Ubiquitin linkage-specific affimers reveal insights into K6-linked ubiquitin signaling. Mol Cell 68:233–246. https://doi.org/10.1016/j.molcel.2017.08.020
37. Wang Y, Ma G, Wang XF, Na L, Guo X, Zhang J, Liu C, Du C, Qi T, Lin Y, Wang X. 2022. Keap1 recognizes EIAV early accessory protein rev to promote antiviral defense. PLoS Pathog 18:e1009986. https://doi.org/10.1371/journal.ppat.1009986
38. Edwards MR, Johnson B, Mire CE, Xu W, Shabman RS, Speller LN, Leung DW, Geisbert TW, Amarasinghe GK, Basler CF. 2014. The marburg virus VP24 protein interacts with Keap1 to activate the cytoprotective antioxidant response pathway. Cell Rep 6:1017–1025. https://doi.org/10.1016/j.celrep.2014.01.043
39. Wyler E, Franke V, Menegatti J, Kocks C, Boltengagen A, Praktiknjo S, Walch-Rückheim B, Bosse J, Rajewsky N, Grässer F, Akalin A, Landthaler M. 2019. Single-cell RNA-sequencing of herpes simplex virus 1-infected cells connects Nrf2 activation to an antiviral program. Nat Commun 10:4878. https://doi.org/10.1038/s41467-019-12894-z
40. Liu B, Fang M, He Z, Cui D, Jia S, Lin X, Xu X, Zhou T, Liu W. 2015. Hepatitis B virus stimulates G6PD expression through HBx-mediated Nrf2 activation. Cell Death Dis 6:e1980. https://doi.org/10.1038/cddis.2015.322
41. Ibrahim MK, Abdelhafez TH, Takeuchi JS, Wakae K, Sugiyama M, Tsuge M, Ito M, Watashi K, El Kassas M, Kato T, Murayama A, Suzuki T, Chayama K, Shimotohno K, Muramatsu M, Aly HH, Wakita T, James Ou J-H. 2021. MafF is an antiviral host factor that suppresses transcription from hepatitis B virus core promoter. J Virol 95. https://doi.org/10.1128/JVI.00767-21
42. Olagnier D, Farahani E, Thyrsted J, Blay-Cadanet J, Herengt A, Idorn M, Hait A, Hernaez B, Knudsen A, Iversen MB, Schilling M, Jørgensen SE, Thomsen M, Reinert LS, Lappe M, Hoang H-D, Gilchrist VH, Hansen AL, Ottosen R, Nielsen CG, Møller C, van der Horst D, Peri S, Balachandran S, Huang J, Jakobsen M, Svenningsen EB, Poulsen TB, Bartsch L, Thielke AL, Luo Y, Alain T, Rehwinkel J, Alcamí A, Hiscott J, Mogensen TH, Paludan SR, Holm CK. 2020. SARS-CoV2-mediated suppression of Nrf2-signaling reveals potent antiviral and anti-inflammatory activity of 4-octyl-Itaconate and dimethyl fumarate. Nat Commun 11:4938. https://doi.org/10.1038/s41467-020-18764-3
43. Patra U, Mukhopadhyay U, Sarkar R, Mukherjee A, Chawla-Sarkar M. 2019. RA-839, a selective agonist of Nrf2/ARE pathway, exerts potent anti-rotaviral efficacy *in vitro*. Antiviral Res 161:53–62. https://doi.org/10.1016/j.antiviral.2018.11.009
44. Huang H, Konduru K, Solovena V, Zhou ZH, Kumari N, Takeda K, Nekhai S, Bavari S, Kaplan GG, Yamada KM, Dhawan S. 2016. Therapeutic potential of the Heme oxygenase-1 inducer hemin against ebola virus infection. Curr Trends Immunol 17:117–123.
45. Huang H, Falgout B, Takeda K, Yamada KM, Dhawan S. 2017. Nrf2-dependent induction of innate host defense via heme oxygenase-1 inhibits zika virus replication. Virology 503:1–5. https://doi.org/10.1016/j.virol.2016.12.019
46. Nio Y, Sasai M, Akahori Y, Okamura H, Hasegawa H, Oshima M, Watashi K, Wakita T, Ryo A, Tanaka Y, Hijikata M. 2019. Bardoxolone methyl as a novel potent antiviral agent against hepatitis B and C viruses in human hepatocyte cell culture systems. Antiviral Res 169:104537. https://doi.org/10.1016/j.antiviral.2019.104537
47. Blight KJ, McKeating JA, Rice CM. 2002. Highly permissive cell lines for subgenomic and genomic hepatitis C virus RNA replication. J Virol 76:13001–13014. https://doi.org/10.1128/jvi.76.24.13001-13014.2002
48. Iwamoto M, Watashi K, Tsukuda S, Aly HH, Fukasawa M, Fujimoto A, Suzuki R, Aizaki H, Ito T, Koiwai O, Kusuhara H, Wakita T. 2014. Evaluation and identification of hepatitis B virus entry inhibitors using HepG2 cells overexpressing a membrane transporter NTCP. Biochem Biophys Res Commun 443:808–813. https://doi.org/10.1016/j.bbrc.2013.12.052
49. Watashi K, Liang G, Iwamoto M, Marusawa H, Uchida N, Daito T, Kitamura K, Muramatsu M, Ohashi H, Kiyohara T, Suzuki R, Li J, Tong S, Tanaka Y, Murata K, Aizaki H, Wakita T. 2013. Interleukin-1 and tumor necrosis factor-alpha trigger restriction of hepatitis B virus infection via a cytidine deaminase activation-induced cytidine deaminase (AID). J Biol Chem 288:31715–31727. https://doi.org/10.1074/jbc.M113.501122
50. Ogura N, Watashi K, Noguchi T, Wakita T. 2014. Formation of covalently closed circular DNA in Hep38.7-Tet cells, a tetracycline inducible hepatitis B virus expression cell line. Biochem Biophys Res Commun 452:315–321. https://doi.org/10.1016/j.bbrc.2014.08.029
51. Sugiyama M, Tanaka Y, Kato T, Orito E, Ito K, Acharya SK, Gish RG, Kramvis A, Shimada T, Izumi N, Kaito M, Miyakawa Y, Mizokami M. 2006. Influence of hepatitis B virus genotypes on the intra- and extracellular expression of viral DNA and antigens. Hepatology 44:915–924. https://doi.org/10.1002/hep.21345
52. Bawono RG, Abe T, Qu M, Kuroki D, Deng L, Matsui C, Ryo A, Suzuki T, Matsuura Y, Sugiyama M, Mizokami M, Shimotohno K, Shoji I. 2021. HERC5 E3 ligase mediates ISGylation of hepatitis B virus X protein to promote viral replication. J Gen Virol 102. https://doi.org/10.1099/jgv.0.001668
53. Kouwaki T, Okamoto T, Ito A, Sugiyama Y, Yamashita K, Suzuki T, Kusakabe S, Hirano J, Fukuhara T, Yamashita A, Saito K, Okuzaki D, Watashi K, Sugiyama M, Yoshio S, Standley DM, Kanto T, Mizokami M, Moriishi K, Matsuura Y. 2016. Hepatocyte factor JMJD5 regulates hepatitis B virus replication through interaction with HBx. J Virol 90:3530–3542. https://doi.org/10.1128/JVI.02776-15
54. Fukutomi K, Hikita H, Murai K, Nakabori T, Shimoda A, Fukuoka M, Yamai T, Higuchi Y, Miyakawa K, Suemizu H, Ryo A, Yamada R, Kodama T, Sakamori R, Tatsumi T, Takehara T. 2022. Capsid allosteric modulators enhance the innate immune response in hepatitis B virus-infected hepatocytes during interferon administration. Hepatol Commun 6:281–296. https://doi.org/10.1002/hep4.1804
55. Murai K, Hikita H, Kai Y, Kondo Y, Fukuoka M, Fukutomi K, Doi A, Yamai T, Nakabori T, Fukuda R, Takahashi T, Miyakawa K, Suemizu H, Ryo A, Yamada R, Kodama T, Sakamori R, Tatsumi T, Takehara T. 2020. Hepatitis C virus infection suppresses hepatitis B virus replication via the RIG-I-like helicase pathway. Sci Rep 10:941. https://doi.org/10.1038/s41598-020-57603-9
56. Deng L, Adachi T, Kitayama K, Bungyoku Y, Kitazawa S, Ishido S, Shoji I, Hotta H. 2008. Hepatitis C virus infection induces apoptosis through a Bax-triggered, mitochondrion-mediated, caspase 3-dependent pathway. J Virol 82:10375–10385. https://doi.org/10.1128/JVI.00395-08
57. Shirakura M, Murakami K, Ichimura T, Suzuki R, Shimoji T, Fukuda K, Abe K, Sato S, Fukasawa M, Yamakawa Y, Nishijima M, Moriishi K, Matsuura Y, Wakita T, Suzuki T, Howley PM, Miyamura T, Shoji I. 2007. E6AP ubiquitin ligase mediates ubiquitylation and degradation of hepatitis C virus core protein. J Virol 81:1174–1185. https://doi.org/10.1128/JVI.01684-06
58. Wertz IE, O'Rourke KM, Zhang Z, Dornan D, Arnott D, Deshaies RJ, Dixit VM. 2004. Human de-etiolated-1 regulates c-Jun by assembling a CUL4A ubiquitin ligase. Science 303:1371–1374. https://doi.org/10.1126/science.1093549
59. Benhenda S, Ducroux A, Rivière L, Sobhian B, Ward MD, Dion S, Hantz O, Protzer U, Michel M-L, Benkirane M, Semmes OJ, Buendia M-A, Neuveut C. 2013. Methyltransferase PRMT1 is a binding partner of HBx and a negative regulator of hepatitis B virus transcription. J Virol 87:4360–4371. https://doi.org/10.1128/JVI.02574-12
60. Hayashi M, Deng L, Chen M, Gan X, Shinozaki K, Shoji I, Hotta H. 2016. Interaction of the hepatitis B virus X protein with the lysine

methyltransferase SET and MYND domain-containing 3 induces activator protein 1 activation. Microbiol Immunol 60:17–25. https://doi.org/10.1111/1348-0421.12345